Gondwana Research 32 (2016) 105–121

Contents lists available at ScienceDirect

Gondwana Research

journal homepage: www.elsevier.com/locate/gr

Phanerozoic amalgamation of the Alxa Block and North China Craton: Evidence from Paleozoic granitoids, U–Pb geochronology and Sr–Nd–Pb–Hf–O isotope geochemistry

Wei Dan [a,b,*], Xian-Hua Li [b], Qiang Wang [a,f,**], Xuan-Ce Wang [b,c,e], Derek A. Wyman [d], Yu Liu [b]

[a] State Key Laboratory of Isotope Geochemistry, Guangzhou Institute of Geochemistry, Chinese Academy of Sciences, Guangzhou, Guangdong 510640, China
[b] State Key Laboratory of Lithospheric Evolution, Institute of Geology and Geophysics, Chinese Academy of Sciences, Beijing 100029, China
[c] ARC Center of Excellence for Core to Crust Fluid Systems (CCFS), Australia
[d] School of Geosciences, The University of Sydney, NSW 2006, Australia
[e] The Institute for Geoscience Research, Department of Applied Geology, Curtin University, Perth, WA 6845, Australia
[f] CAS Center for Excellence in Tibetan Plateau Earth Sciences

ARTICLE INFO

Article history:
Received 2 September 2014
Received in revised form 1 February 2015
Accepted 13 February 2015
Available online 18 March 2015

Handling Editor: W.J. Xiao

Keywords:
North China Craton
Alxa Block
Cryptic suture zone
High $\delta^{18}O$ zircon
Zircon Hf–O isotopes

ABSTRACT

The North China Craton (NCC) has been considered to be part of the supercontinent Columbia. The nature of the NCC western boundary, however, remains strongly disputed. A key question in this regard is whether or not the Alxa Block is a part of the NCC. It is located in the vicinity of the inferred boundary, and therefore could potentially resolve the issue of the NCC's relationship to the Columbia supercontinent. Some previous studies based on the Alxa Block's geological evolution and detrital zircon ages suggested that it is likely not a part of the NCC. The lack of evidence from key igneous rock units, however, requires further constraints on the tectonic affinity of the western NCC and Alxa Block and on the timing of their amalgamation.

In this study, new zircon U–Pb age and Hf–O isotopes and whole-rock geochemical and Sr–Nd–Pb isotopic data for the Paleozoic granitoids in or near the eastern Alxa Block were used to constrain the petrogenesis of these rocks and the relationship between the Alxa Block and NCC. Secondary ion mass spectrometry (SIMS) U–Pb zircon dating indicates that the Bayanbulage, Hetun, Diebusige and South Diebusige granitoids were formed at ca. 423 Ma, 345 Ma, 345 Ma and 337 Ma, respectively. The Late Silurian (Bayanbulage) quartz diorites have variable SiO_2 (58.0–67.9 wt.%), and low Sr/Y (20–24) values, while the Early Carboniferous (Hetun, Diebusige and South Diebusige) monzogranites have high SiO_2 (71.5–76.7 wt.%) and Sr/Y (40–94) values. The Late Silurian quartz diorites display relatively homogeneous and high zircon $\delta^{18}O$ (8.5–9.1‰) and $\varepsilon_{Hf}(t)$ (−8.6 to −5.3) values, high whole-rock $\varepsilon_{Nd}(t)$ values (−9.2 to −7.6) and highly radiogenic Pb isotopes ($^{206}Pb/^{204}Pb$ = 18.13–18.25), whereas the Early Carboniferous monzogranites exhibit relatively low and variable zircon $\delta^{18}O$ (5.7–7.2‰) and $\varepsilon_{Hf}(t)$ (−23.1 to −7.4) values, low whole-rock initial $^{87}Sr/^{86}Sr$ (0.7043–0.7070) and $\varepsilon_{Nd}(t)$ (−19.1 to −13.5) values and variable Pb isotopes ($^{206}Pb/^{204}Pb$ = 16.06–18.22). The differences in whole rock Nd model ages and Pb isotope compositions of the Paleoproterozoic–Permian rocks in either side of the west fault of the Bayanwulashan–Diebusige complexes suggest that the Alxa Block is not a part of the NCC, and that the western boundary of the NCC is probably located on this fault. Furthermore, the linear distribution of the Early Paleozoic–Early Carboniferous granitoids, the high zircon $\delta^{18}O$ values of the Late Silurian quartz diorites, the Early Devonian metamorphism and the foreland basin system formed during the collision between the Alxa Block and the NCC indicate that a Paleozoic cryptic suture zone likely existed in this area and records the amalgamation of the Alxa Block and North China Craton. Together with detrital zircon data, the initial collision was considered to have possibly occurred in Late Ordovician.

1. Introduction

Continent–continent or arc–continental collisions commonly produce orogens that are marked by linear zones of igneous rocks accompanied by typical marker lithologies (i.e., high-pressure metamorphic rocks and ophiolites), and the Cenozoic Himalaya Orogen is a classic example (e.g., Yin and Harrison, 2000). In some cases, however, cryptic suture zones are only marked by linear distributions of igneous

* Correspondence to: W. Dan, State Key Laboratory of Isotope Geochemistry, Guangzhou Institute of Geochemistry, Chinese Academy of Sciences, Guangzhou, Guangdong 510640, China. Tel.: +86 20 85292986; fax: +86 20 85290130.
** Corresponding author. Tel: +86 20 85290277; fax: +86 20 85290130.
E-mail addresses: danwei@gig.ac.cn (W. Dan), wqiang@gig.ac.cn (Q. Wang).

http://dx.doi.org/10.1016/j.gr.2015.02.011
1342-937X/

rocks at the contact zones between two amalgamated blocks, as is the case for the Mesozoic granitoid zone between the Yangtze and Cathaysia blocks (Wong et al., 2011), the Mesozoic granitoid zone between the North China Craton and Yangtze Block (e.g., Su et al., 2013), and Mesoproterozoic granitoids stitching three terranes in the SW Grenville Province (Peck et al., 2004). These studies demonstrate that a granitoid zone with two geochemically contrasting sub-zones can be used to define the location of a cryptic suture zone, especially when no metamorphic rocks or ophiolites are found in the inferred suture zone.

The North China Craton (NCC) is one of the world's major cratons (Bleeker, 2003). It is the largest in China while also being one of the oldest, based on the presence of ≥3.8 Ga crustal materials (e.g., Liu et al., 1992; Wu et al., 2008a) within the more abundant ca. 2.5 Ga and 1.8 Ga rocks (e.g., Zhao et al., 2005; Zhao and Cawood, 2012; Zhao and Zhai, 2013; Zheng et al., 2013; Zhao, 2014). Its evolutionary history is critical for the understanding of the assembly and break-up of Columbia because very different models have been proposed for its location in the supercontinent (e.g., Zhao et al., 2002, 2004; Kusky et al., 2007; Hou et al., 2008; Kusky and Santosh, 2009; Rogers and Santosh, 2009; Meert, 2012; Roberts, 2013; Teixeira et al., 2013; Nance et al., 2014; Wang et al., 2015). However, its western boundary remains strongly disputed (e.g., Dong et al., 2007; Dan et al., 2012; Gong et al., 2012; Dan et al., 2014a), hampering a better understanding of its position in the supercontinent. It is widely accepted that the Alxa Block (Fig. 1) represents the westernmost part of the NCC (e.g., Zhai et al., 2000; Zhao et al., 2005; Dong et al., 2007; Geng et al., 2010; Gong et al., 2012). These models, however, appear inconsistent with the newly-identified ca. 2.3 Ga and ca. 0.9 Ga magmatic events in the eastern Alxa Block (Dan et al., 2012, 2014a) because similarly-aged rocks have not been reported within the Western Block of the NCC (Dan et al., 2012). It has also been suggested that the models are not consistent with the different age distribution patterns of detrital zircon grains between the westernmost NCC and the Alxa Block (Zhang et al., 2011; Dan et al., 2014a; Yuan and Yang, 2015a). However, a lack of recognized magmatic events in key areas requires that further studies be undertaken to fully resolve the tectonic affinities of the two blocks and to constrain the timing of their amalgamation.

In this study, we present in situ zircon U–Pb age and Hf–O isotopic compositions along with whole-rock element and Sr–Nd–Pb isotopic compositions for the newly-identified Paleozoic quartz diorites and high Sr/Y monzogranites in the vicinity of the eastern Alxa Block. The aim of this work is to (1) place geochronological and geochemical constrains on the timing and petrogenesis of the Paleozoic granitoids, (2) examine the relationship of the Alxa Block and the NCC and (3) shed light on the timing of the Alxa Block amalgamation with the NCC to form a single block.

2. Geological background and sample descriptions

The North China Craton (NCC) is bounded by the Central Asian Orogenic Belt (CAOB) to the north, the Sulu ultrahigh-pressure (UHP) metamorphic belt to the east and the Qinling–Dabie orogenic belt to the south (Fig. 1). It has been divided into four Archean continental blocks (i.e., the Longgang, Langrim, Yinshan and Ordos blocks) and three Paleoproterozoic mobile belts: the Khondalite Belt, the Trans-North China Orogen and the Jiao–Liao–Ji Belt (e.g., Zhao et al., 2005; Zhao and Cawood, 2012; Zhao and Zhai, 2013; Zheng et al., 2013; Zhao, 2014). It is generally accepted that the NCC was assembled during the Late Paleoproterozoic (1900–1850 Ma) (e.g., Kusky and Li, 2003; Zhao et al., 2005; Zhai and Santosh, 2011; Zhao and Cawood, 2012; Zhao et al., 2012; Zhao, 2014). After cratonization, it remained stable until the Late Paleozoic, although several intraplate or rift-related magmatic episodes took place between the Late Paleoproterozoic and Paleozoic times (Peng et al., 2011 and references there in). The eastern NCC has been mobilized and modified since the Early Mesozoic, resulting in widespread occurrence of magmatism, crustal deformation and lithospheric thinning (e.g., Wu et al., 2008b and references therein).

The Alxa Block, located in the westernmost part of North China, is generally thought to be the westernmost part of the NCC (e.g., Zhai et al., 2000; Zhao et al., 2005; Gong et al., 2012), although J.X. Zhang

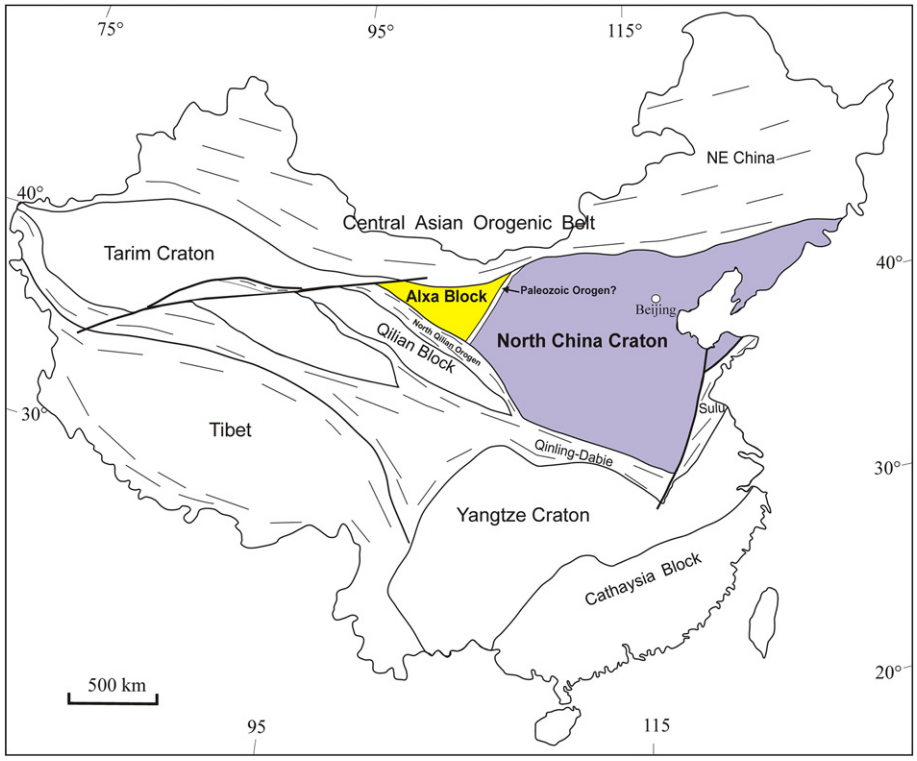

Fig. 1. The Alxa Block in the tectonic framework of China, and the tectonic subdivision of the North China Craton. Modified from Zhao and Cawood (2012).

et al. (2013a,b and references therein) proposed that the craton extends further west to include the Dunhuang block, Tarim Craton. The Alxa Block is largely covered by Cenozoic sediments, and outcrops of pre-Neoproterozoic crystalline basement rocks are only documented in the southwestern and eastern parts of the block (Fig. 2 in Dan et al., 2012; Gong et al., 2012; J.X. Zhang et al., 2013a). The Diebusige and Bayanwulashan complexes (Fig. 2), traditionally considered to be parts of the eastern Alxa Block, were thought to be Archean basement rocks (NMBGMR, 1991). Our recent work, however, demonstrated that these complexes formed during the Early Paleoproterozoic, and underwent two metamorphic events at ~1.90 Ga and ~1.80 Ga (Dan et al., 2012). In the Neoproterozoic, a few 930–910 Ma S-type granites were intruded into the central Alxa Block (Dan et al., 2014a).

The oldest Phanerozoic sedimentary rocks occur in the Upper Carboniferous–Lower Permian Amushan Formation, mainly in the northern Alxa Block (Fig. 2). A notable feature of the Alxa Block is the large volume of Phanerozoic granitoids (NMBGMR, 1991) that mainly formed between 320 Ma and 260 Ma (Fig. 2) (Dan et al., 2014b and references therein). Igneous rocks with ages >320 Ma are very rare, apart from a few ~447 Ma intermediate-felsic volcanic rocks and ~394 Ma diorites reported in the eastern Alxa Block (Fig. 2) (Li, 2006). However, the corresponding petrological and geochemical data are relatively limited, which hampers a better understanding of their petrogenesis.

In this study, we analyzed granitoids collected from the Diebusige, South Diebusige, Bayanbulage and Hetun areas (Figs. 2 and 3), all of which were located near the potential boundary between the NCC and the Alxa Block (Dan et al., 2012), and have been considered to be a part of the Alxa Block. The Bayanbulage gneissic quartz diorites show strong deformation and are composed of plagioclase (60–70 vol.%), biotite (15–20 vol.%), quartz (10–20 vol.%), as well as minor apatite and zircon. The Hetun monzogranites, located adjacent to the Bayanwulashan Complex, have medium-grained texture, consisting of plagioclase (40–45 vol.%), K-feldspar (25–30 vol.%), quartz (25–30 vol.%), biotite (~2 vol.%), as well as minor apatite and zircon. The monzogranites collected from the Diebusige and South Diebusige consist of plagioclase (30–40 vol.%), K-feldspar (30–35 vol.%), quartz (20–30 vol.%), biotite (2–8 vol.%) and minor accessory minerals.

3. Analytical procedures

3.1. Zircon U–Pb dating

Isotopic analyses of U, Th and Pb were conducted using the Cameca IMS-1280 SIMS at the Institute of Geology and Geophysics, Chinese Academy of Sciences (IGG-CAS), Beijing, using operating and data processing procedures similar to those described by Li et al. (2010a). Uncertainties on individual analyses in the data tables are reported at a 1σ level. Mean ages for pooled U/Pb and Pb/Pb analyses are quoted with 2σ and/or 95% confidence intervals. The weighted mean U–Pb ages and Concordia plots were processed using Isoplot/Ex v. 3.0 program (Ludwig, 2003). SIMS zircon U–Pb isotopic data are presented in Appendix 1.

The LA-ICP-MS U-Pb dating for sample 09AL131 was conducted using an Agilent 7500a ICP-MS with an attached 193 nm excimer ArF laser-ablation system (GeoLas Plus) at IGG-CAS. The analytical procedures are similar to those described by Xie et al. (2008). $^{207}Pb/^{206}Pb$ and $^{206}Pb/^{238}U$ ratios were calculated using the ICPMSDataCal software (Liu et al., 2010), using the zircon standard 91500 as an external standard. Common Pb was corrected according to the method proposed by Andersen (2002). The weighted mean U–Pb ages and Concordia plots were processed using Isoplot/Ex v. 3.0 program (Ludwig, 2003). Analyses of the zircon standard GJ-1 as an unknown yielded a weighted mean $^{206}Pb/^{238}U$ age of 606 ± 4 Ma (2σ, n = 8), which is in good agreement with the recommended value (Jackson et al., 2004). LA-ICP-MS zircon U–Pb isotopic data are presented in Appendix 1.

3.2. Zircon oxygen isotopes

Zircon oxygen isotopes were measured using the same Cameca IMS-1280 SIMS at IGG-CAS. The detailed analytical procedures were similar to those described by Li et al. (2010a). The measured oxygen isotopic data were corrected for instrumental mass fractionation (IMF) using the Penglai zircon standard ($\delta^{18}O_{VSMOW}$ = 5.3‰) (Li et al., 2010b). The internal precision of a single analysis generally was better than 0.2‰ (1σ standard error) for the $^{18}O/^{16}O$ ratio. The

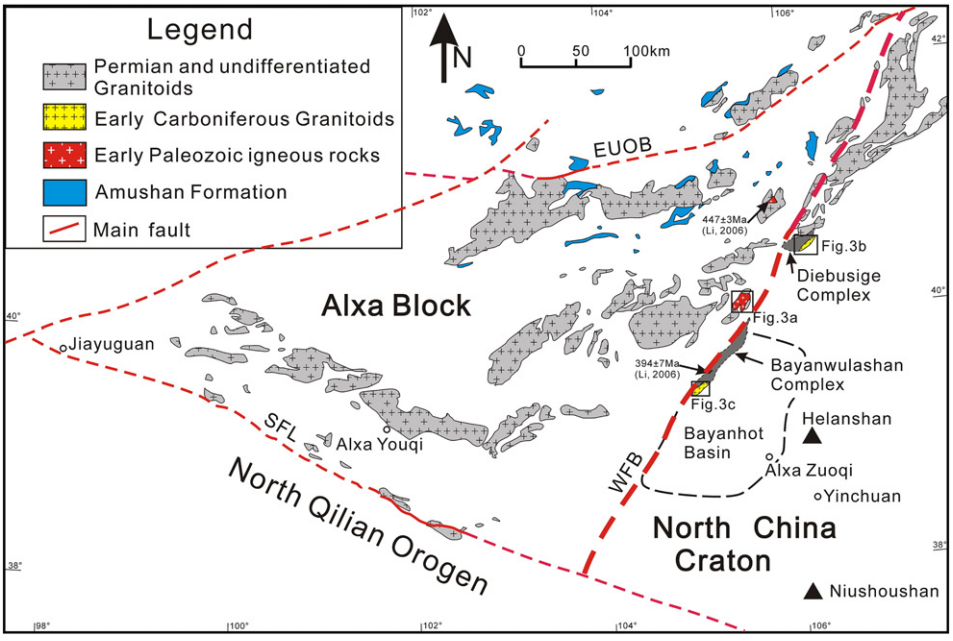

Fig. 2. Geological map showing the distribution of Phanerozoic granitoids in the Alxa Block and adjacent areas. The studied granitoids are near the proposed boundary between the North China Craton and Alxa Block. SFL, southern margin fault of Longshoushan; WFB, western margin fault of Bayanwulashan; EUOB, Enger Us Ophiolite Belt.
Modified from Dan et al. (2014b).

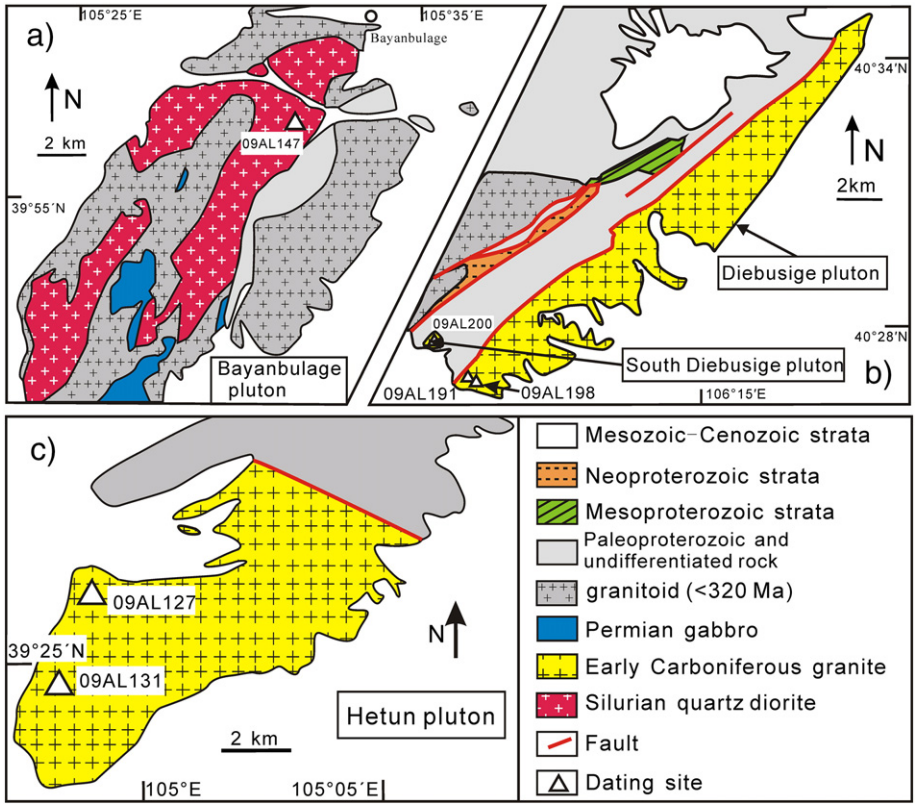

Fig. 3. Geological sketch-map of the (a) Bayanbulage, (b) Hetun and (c) Diebusige areas, with locations of dating samples. Modified after NMBGMR (1991).

external precision, measured by the reproducibility of repeated analyses of Penglai standard, is 0.50‰ (2SD, n = 68). Ten measurements of the 91500 zircon standard during the course of this study yielded a weighted mean of $\delta^{18}O = 10.2 \pm 0.5‰$ (2SD), which is consistent within errors with the reported value of 9.9 ± 0.3‰ (Wiedenbeck et al., 2004). Zircon oxygen isotopic data are listed in Appendix 2.

3.3. Zircon Lu–Hf isotopes

In situ zircon Lu–Hf isotopic analyses were carried out on a Neptune multi-collector ICP-MS equipped with a Geolas-193 laser-ablation system at IGG-CAS. Lu–Hf isotopic analyses were conducted on the same zircon grains that were previously analyzed for U–Pb and O isotopes. Detailed analytical procedures were similar to those described by Wu et al. (2006). Measured $^{176}Hf/^{177}Hf$ ratios were normalized to $^{179}Hf/^{177}Hf = 0.7325$. Further external adjustment was not applied for the unknowns because our determined $^{176}Hf/^{177}Hf$ ratios for zircon standards 91500 (0.282309 ± 0.000004) and GJ-1 (0.282000 ± 0.000008) were in good agreement within errors with the reported values (Wu et al., 2006). Zircon Hf isotopic data are listed in Appendix 2.

3.4. Major and trace elements

Sixteen rock samples powdered to ~200-mesh size were used for geochemical analyses. Major element oxides were analyzed on fused glass beads using a Rigaku RIX 2000 X-ray fluorescence spectrometer at the State Key Laboratory of Isotope Geochemistry, the Guangzhou Institute of Geochemistry, Chinese Academy of Sciences (SKLaBIG GIG CAS). Calibration lines used in quantification were produced by bivariate regression of data from 36 reference materials encompassing a wide range of silicate compositions (Li et al., 2005). Analytical uncertainties are between 1% and 5%. Trace elements were analyzed using an Agilent 7500a ICP-MS at GIG-CAS. Analytical procedures were similar to those described by Li et al. (2000). A set of USGS and Chinese national rock standards, including BHVO-2, GSR-1, GSR-2, GSR-3, AGV-2, W-2 and SARM-4 were chosen for calibration. Analytical precision typically is better than 5%. Geochemical results are listed in Table 1.

3.5. Sr–Nd–Pb isotopic compositions

Sr–Nd–Pb isotopic compositions were determined using a Micromass Isoprobe multi-collector ICP-MS at SKLaBIG GIG CAS. Sr and Nd were separated using cation columns, and Nd fractions were further separated by HDEHP-coated Kef columns. Detailed analytical procedures were described by Li et al. (2004). The measured $^{87}Sr/^{86}Sr$ ratio of the NBS 987 standard and $^{143}Nd/^{144}Nd$ ratio of the JNdi-1 standard were 0.710274 ± 18 (n = 11, 2σ) and 0.512093 ± 11 (n = 11, 2σ), respectively. All measured Nd and Sr isotope ratios were normalized to $^{146}Nd/^{144}Nd = 0.7219$ and $^{86}Sr/^{88}Sr = 0.1194$, respectively. For Pb isotope determinations, about 50 mg powder was weighed into a Teflon beaker and dissolved in concentrated HF at 180C for 3 days. Lead was separated and purified by conventional cation-exchange techniques with diluted HBr as an eluant. Total procedural blanks were less than 50 pg Pb. Measurement of Pb isotopic compositions were carried out following procedures described by Zhu et al. (2001). Repeated analyses of NBS 981 yielded average values of $^{206}Pb/^{204}Pb = 16.936$, $^{207}Pb/^{204}Pb = 15.487$ and $^{208}Pb/^{204}Pb = 36.677$. The Sr–Nd–Pb isotope results for whole rocks of ten samples are listed in Table 2.

Table 1
Geochemical data for the Paleozoic granitoids near eastern Alxa Block.

Rock type	Hetun monzogranite						Bayanbulage quartz diorite		Bayanbulage	Diebusige monzogranite			South Diebusige monzogranite		
Sample no.	09AL127	09AL128	09AL129	09AL130	09AL131	09AL132	09AL147	09AL148	09AL149	09AL191	09AL198	09AL199	09AL200	09AL201	09AL202
Major elements (wt.%)															
SiO_2	76.36	72.64	74.64	64.03	73.75	72.64	57.17	62.55	67.27	71.82	70.10	70.72	73.99	72.16	74.32
TiO_2	0.06	0.16	0.13	0.20	0.12	0.14	1.07	0.84	0.53	0.29	0.33	0.33	0.18	0.32	0.15
Al_2O_3	13.50	14.78	13.71	16.94	14.35	14.96	16.20	16.57	15.74	14.78	14.76	14.98	13.34	14.06	13.44
$Fe_2O_3^T$	0.48	1.30	1.20	2.61	1.11	1.20	7.78	6.82	4.35	1.94	2.35	2.30	1.53	2.77	1.19
MnO	0.04	0.04	0.04	0.10	0.05	0.03	0.19	0.11	0.06	0.03	0.03	0.03	0.02	0.03	0.02
MgO	0.18	0.55	0.52	0.87	0.45	0.48	2.94	1.77	1.33	0.71	0.81	0.83	0.30	0.52	0.24
CaO	0.73	1.70	1.60	3.04	1.27	1.52	5.74	3.81	3.48	1.41	1.57	1.34	1.24	1.58	1.47
Na_2O	4.02	3.72	3.58	1.68	3.65	4.08	3.82	3.40	3.47	3.25	3.37	3.14	2.59	3.06	2.91
K_2O	4.47	4.54	4.19	6.21	4.62	4.33	2.85	2.74	2.59	4.86	4.82	5.01	5.80	4.51	5.33
P_2O_5	0.01	0.06	0.08	0.06	0.03	0.04	0.46	0.28	0.19	0.06	0.07	0.07	0.03	0.07	0.03
L.O.I	0.39	0.66	0.44	4.26	0.75	0.75	1.48	0.93	0.93	0.94	1.88	1.33	0.98	0.96	1.02
Total	100.23	100.15	100.14	100.00	100.16	100.17	99.72	99.93	99.82	100.09	100.08	100.07	100.00	100.03	100.09
Mg#	45.0	48.3	48.8	42.3	47.2	47.1	45.4	36.3	40.2	44.6	43.1	44.2	30.1	29.1	30.7
A/CNK	1.06	1.05	1.03	1.13	1.08	1.06	0.82	1.07	1.06	1.12	1.08	1.15	1.04	1.10	1.02
Trace element (ppm)															
Sc	3.63	3.52	3.11	4.50	2.19	2.42	25.0	10.1	11.4	3.64	4.60	4.27	2.27	4.57	1.91
V	9.23	20.8	18.5	40.5	20.7	20.9	123	45.0	66.7	30.5	38.9	36.7	5.53	18.8	5.17
Cr	14.8	25.0	23.5	29.4	28.4	30.6	59.1	26.8	32.2	10.3	12.7	11.6	2.31	0.86	0.065
Ni	5.11	7.34	7.05	11.82	9.93	9.88	20.0	7.51	6.79	1.43	1.76	1.61	3.58	0.82	0.34
Ga	16.9	16.4	14.9	26.6	16.2	16.8	25.3	22.5	24.5	16.5	16.3	16.7	11.9	14.7	11.9
Rb	118	101	90.3	185	99.4	94.7	154	110	140	94.5	109	95.6	56.5	60.1	48.8
Sr	103	488	488	448	373	403	704	333	472	332	276	375	405	476	413
Y	10.9	11.2	9.14	14.1	4.70	4.30	29.6	16.0	23.1	7.30	9.69	9.43	6.84	8.14	7.71
Zr	56.7	73.0	73.2	96.2	64.5	87.0	234	236	312	143	163	166	158	175	154
Nb	18.9	26.2	15.7	28.2	35.7	19.5	14.2	14.6	14.8	11.2	8.55	8.34	3.45	6.21	2.86
Ba	278	1104	1039	1613	755	777	801	561	918	2119	2374	2452	2865	2877	2832
La	6.64	27.9	26.2	20.0	13.4	16.1	32.4	41.4	22.0	39.3	39.8	42.6	47.1	34.5	47.7
Ce	14.3	48.0	45.0	34.7	24.0	28.4	69.9	82.7	43.9	64.5	65.1	71.9	85.9	60.9	87.5
Pr	1.74	4.86	4.49	3.59	2.43	2.89	9.45	10.1	5.68	6.16	6.40	6.77	9.58	6.75	9.79
Nd	6.73	15.6	14.5	11.6	7.61	9.23	37.9	36.0	21.1	20.8	22.0	22.8	37.4	26.4	38.3
Sm	2.05	2.68	2.33	2.04	1.28	1.38	8.55	6.47	4.78	3.01	3.23	3.11	6.23	4.26	6.58
Eu	0.38	0.73	0.66	0.67	0.39	0.50	2.10	1.27	1.60	0.73	0.84	0.79	1.52	1.47	1.51
Gd	1.87	2.38	2.03	2.03	1.03	1.13	7.34	5.21	4.62	2.04	2.33	1.95	3.81	2.84	3.92
Tb	0.31	0.33	0.28	0.29	0.13	0.13	1.08	0.67	0.77	0.26	0.30	0.22	0.41	0.33	0.42
Dy	1.93	1.84	1.52	1.74	0.75	0.65	6.03	3.49	4.60	1.29	1.52	1.02	1.71	1.57	1.72
Ho	0.41	0.39	0.32	0.43	0.17	0.13	1.22	0.65	0.94	0.22	0.26	0.17	0.24	0.25	0.25
Er	1.11	1.13	0.91	1.21	0.54	0.46	3.12	1.62	2.44	0.60	0.73	0.45	0.63	0.67	0.63
Tm	0.18	0.17	0.14	0.21	0.11	0.080	0.42	0.21	0.32	0.10	0.13	0.076	0.10	0.11	0.10
Yb	1.27	1.27	0.92	1.61	0.87	0.69	2.79	1.26	1.96	0.64	0.84	0.52	0.66	0.70	0.66
Lu	0.20	0.21	0.16	0.26	0.16	0.13	0.44	0.20	0.29	0.11	0.15	0.092	0.13	0.12	0.12
Hf	2.70	2.39	2.36	3.13	2.67	2.94	5.42	5.77	7.01	3.86	4.10	4.27	4.58	4.41	4.45
Ta	1.68	2.08	0.99	1.89	4.20	1.21	0.91	0.80	1.06	0.95	0.57	0.52	0.11	0.15	0.09
Pb	46.5	70.0	69.7	205	90.7	79.1	15.9	19.8	16.4	27.3	15.2	21.2	18.5	17.6	18.0
Th	9.17	12.7	9.73	14.4	11.2	11.8	8.38	16.3	10.4	6.05	6.76	7.09	2.79	1.47	2.94
U	2.14	3.74	2.90	1.37	2.91	1.95	2.91	2.42	2.41	0.80	0.60	0.53	0.14	0.16	0.15
Sr/Y	9	44	53	32	79	94	24	21	20	45	28	40	59	59	54

Mg# = 100 × molar Mg^{2+} / (Mg^{2+} + Fe^{2+}), assuming FeO / (FeO + Fe_2O_3) = 0.9; A / CNK = molar Al_2O_3 / (CaO + Na_2O + K_2O).

Table 2
Whole rock Sr–Nd–Pb data for the Paleozoic granitoids near the eastern Alxa Block.

Sample	$^{87}Rb/^{86}Sr$	$^{87}Sr/^{86}Sr$	±2σ	$(^{87}Sr/^{86}Sr)_i$	$^{147}Sm/^{144}Nd$	$^{143}Nd/^{144}Nd$	±2σ	$\varepsilon_{Nd}(t)$	T_{DM} (Ma)	T_{2DM} (Ma)	$^{206}Pb/^{204}Pb$	$^{207}Pb/^{204}Pb$	$^{208}Pb/^{204}Pb$
Ca. 423 Ma Bayanbulage quartz diorite													
09AL147	0.631	0.714524	0.000013	0.71072	0.1362	0.512000	0.000007	−9.2	2259	1910	18.246	15.558	38.349
09AL148	0.957	0.713042	0.000014	0.70728	0.1087	0.512007	0.000007	−7.6	1659	1780	18.132	15.542	38.469
Ca. 345 Ma Hetun monzogranite													
09AL127	3.55	0.721760	0.000013	0.70432	0.1838	0.511761	0.000006	−16.6	6998	2419	17.259	15.411	37.007
09AL128	0.642	0.709308	0.000013	0.70616	0.1036	0.511731	0.000007	−13.6	1964	2208	17.780	15.483	37.494
09AL130	1.29	0.711173	0.000016	0.70482	0.1060	0.511738	0.000009	−13.6	1997	2204	17.665	15.478	37.474
09AL131	0.878	0.710984	0.000016	0.70667	0.1017	0.511731	0.000007	−13.5	1930	2201	18.219	15.511	37.571
Ca. 345 Ma Diebusige monzogranite													
09AL191	0.823	0.710026	0.000017	0.70598	0.0874	0.511410	0.000012	−19.1	2096	2657	16.227	15.303	36.222
09AL198	1.15	0.710549	0.000020	0.70491	0.0888	0.511424	0.000007	−19.0	2103	2641	16.359	15.318	36.385
Ca. 337 Ma South Diebusige monzogranite													
09AL200	0.442	0.708936	0.000011	0.70682	0.1005	0.511503	0.000006	−18.0	2215	2558	16.070	15.283	36.152
09AL202	0.342	0.708668	0.000016	0.70703	0.1037	0.511504	0.000008	−18.1	2278	2568	16.057	15.282	36.168

$(^{87}Sr/^{86}Sr)_i = (^{87}Sr/^{86}Sr) - (^{87}Rb/^{86}Sr) \times (e^{\lambda t} - 1)$; $\lambda_{Rb-Sr} = 0.0142\ Ga^{-1}$; $\varepsilon_{Nd}(t) = 10{,}000 \times \{[(^{143}Nd/^{144}Nd)_s - (^{147}Sm/^{144}Nd)_s \times (e^{\lambda t} - 1)] / [(^{143}Nd/^{144}Nd)_{CHUR,0} - (^{147}Sm/^{144}Nd)_{CHUR} \times (e^{\lambda t} - 1)] - 1\}$; $T_{DM} = 1/\lambda \times \ln\{1 + [(^{143}Nd/^{144}Nd)_s - (^{143}Nd/^{144}Nd)_{DM}] / [(^{147}Sm/^{144}Nd)_s - (^{147}Sm/^{144}Nd)_{DM}]\}$; $T_{2DM} = T_{DM} - (T_{DM} - t)((f_c - f_s) / (f_c - f_{DM}))$; $f_{Sm/Nd} = (^{147}Sm/^{144}Nd)_s/(^{147}Sm/^{144}Nd)_{CHUR} - 1$; where f_c, f_s and f_{DM} are the $f_{Sm/Nd}$ values of the continental crust, sample and the depleted mantle; $f_c = -0.4$, $f_{DM} = 0.08592$; t = crystallization time; $(^{147}Sm/^{144}Nd)_s$ and $(^{143}Nd/^{144}Nd)_s$ are values of analyzed sample; $(^{147}Sm/^{144}Nd)_{CHUR} = 0.1967$ and $(^{143}Nd/^{144}Nd)_{CHUR,0} = 0.512638$; $(^{147}Sm/^{144}Nd)_{DM} = 0.2135$ and $(^{143}Nd/^{144}Nd)_{DM} = 0.51315$; $(^{147}Sm/^{144}Nd)_c = 0.118$; $\lambda_{Sm-Nd} = 0.00654\ Ga^{-1}$.

4. Results

4.1. Zircon U–Pb dating results

Zircon grains selected for U–Pb dating were mostly euhedral to subhedral, with lengths of ~100–250 μm, and length to width ratios of 2:1 to 4:1. The oscillatory zoning revealed in CL images for most grains (Fig. 4) and high Th/U ratios (0.15–0.68) suggest a magmatic origin (Belousova et al., 2002). U–Pb Concordia diagrams are shown in Fig. 5, and U–Pb age data are given in Appendix 1.

4.1.1. The Bayanbulage pluton

Seventeen zircon spot analyses from a quartz diorite sample (09AL147) yield a weighted mean $^{206}Pb/^{238}U$ age of 423 ± 3 Ma (MSWD = 1.1, 95% confidence interval) (Fig. 5a), which is interpreted as the crystallization age of the Bayanbulage quartz diorites.

4.1.2. The Hetun pluton

Two of the Hetun monzogranites (09AL131 and 09AL127) were dated. Nine zircon spots were analyzed for sample 09AL131, and they have high U contents up to ~5000 ppm (Appendix 1). Almost all these analyses show variable discordance, and the degree of discordance is apparently correlated directly with U contents (not shown), indicating radiogenic Pb loss, probably due to radiation damage. They yield an upper intercept age of 366 ± 16 Ma (MSWD = 0.81) (Fig. 5b), which is interpreted as the approximate crystallization age of this sample. Fifteen analyses were obtained from sample 09AL127, yielding a wide range of $^{206}Pb/^{238}U$ ages from 368 Ma to 338 Ma. These ages can be unmixed into two pools, i.e., 362 ± 6 Ma and 345 ± 4 Ma (Fig. 5c).

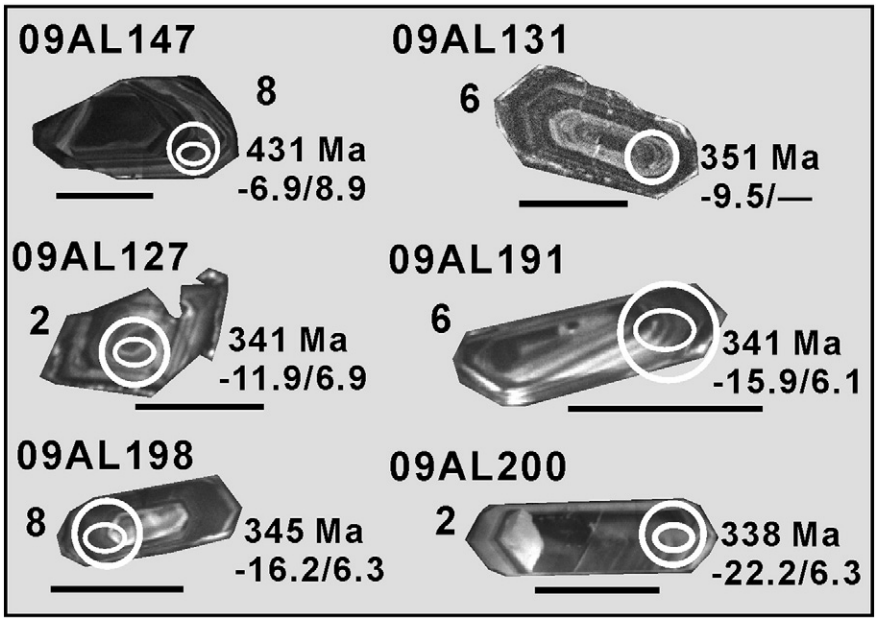

Fig. 4. Cathodoluminescence images of representative zircons for in situ analyses of U–Pb and/or Hf–O isotopes. Small ellipses indicate the SIMS analytical spots for U–Pb and/or O isotopes, and large circles denote the LA-(MC) ICP-MS analytical spots for Lu–Hf or U–Pb isotopes. Numbers near the analysis spots are the U–Pb ages (Ma) and $\varepsilon_{Hf}(t)/\delta^{18}O$ values. The black scale bars are 100 μm long.

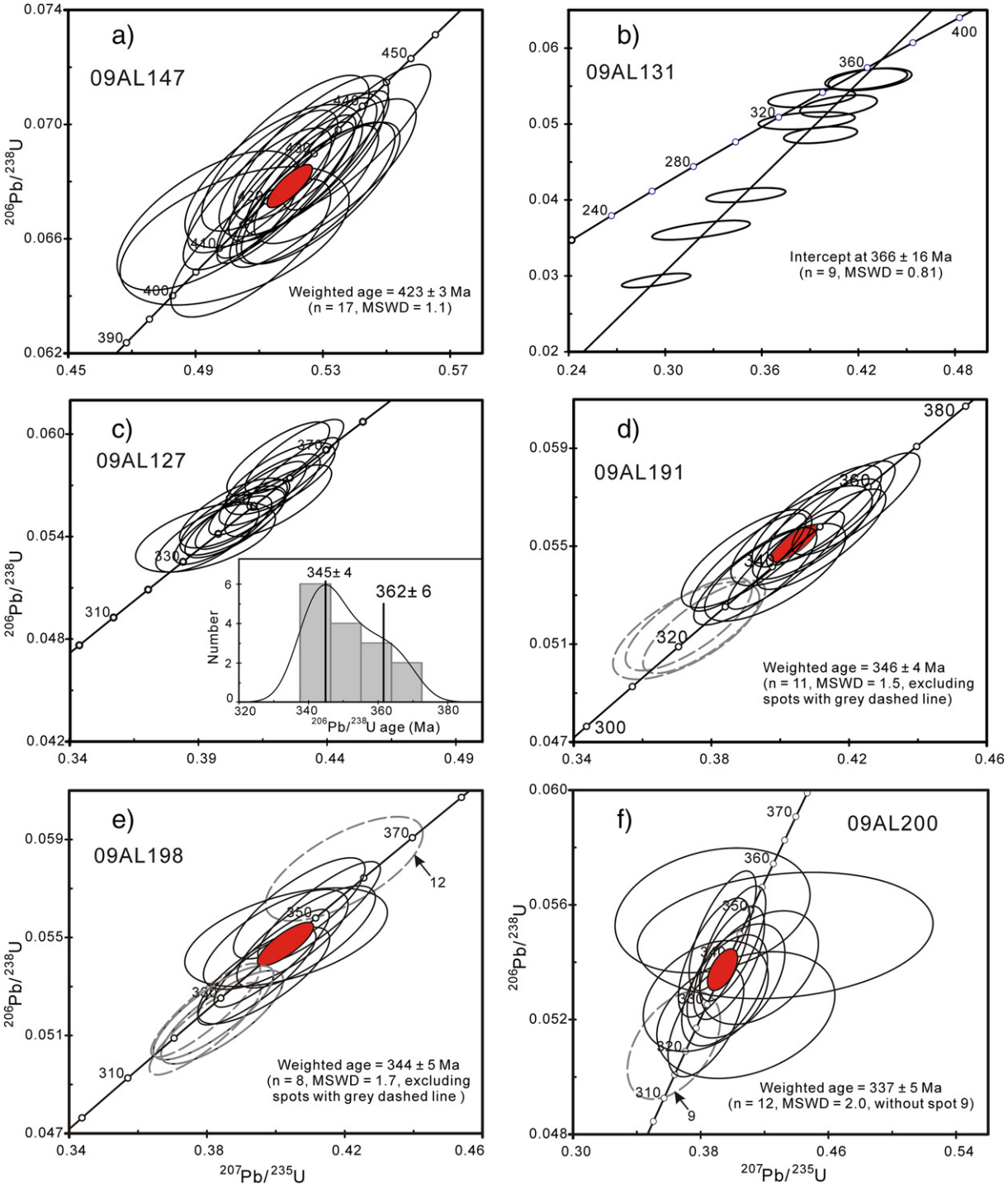

Fig. 5. In situ U–Pb dating results for the Paleozoic rocks. (a) Quartz diorite from Bayanbulage pluton (09AL147), (b, c) monzogranites from Hetun pluton (09AL131 and 09AL127), (c, d) monzogranites from Diebusige pluton (09AL191 and 09AL198), (f) monzogranites from Diebusige pluton (09AL200). Data-point error ellipses are 2σ.

The former is interpreted as an older igneous event recorded in xenocrystic zircons, and the latter as the crystallization age of this sample. Thus, both samples yield similar crystallization ages. Owing to the relatively large error in the age of sample 09AL131, the age of 345 ± 4 Ma from sample 09AL127 was considered as the crystallization age of the Hetun monzogranites.

4.1.3. The Diebusige pluton

Two of the Diebusige monzogranites (09AL191 and 09AL198) were dated. Fourteen zircon spot analyses from sample 09AL191 show a wide range of $^{206}Pb/^{238}U$ ages varying from 356 Ma to 324 Ma. Eleven of fourteen analyses yield a weighted mean age of 346 ± 4 Ma (MSWD = 1.5, 95% confidence interval), which is interpreted as the crystallization age of sample 09AL191. The remaining three analyses show slightly younger ages than the main population (Fig. 5d), probably due to radiogenic Pb loss. Thirteen zircon spot analyses from sample 09AL198 exhibit a wide range of $^{206}Pb/^{238}U$ ages varying from 362 Ma to 322 Ma. Eight analyses with $^{206}Pb/^{238}U$ ages of 352–335 Ma yield a weighted mean age of 344 ± 5 Ma (MSWD = 1.7, 95% confidence interval), which is interpreted as the crystallization age of this sample.

One analysis with $^{206}Pb/^{238}U$ age of 362 Ma was interpreted as a xenocrystic zircon, and the remaining four analyses show slightly younger ages than the main population (Fig. 5e), probably due to radiogenic Pb loss. Thus, the Diebusige monzogranites crystallized at ca. 345 Ma.

4.1.4. The South Diebusige pluton

Twelve of the total thirteen analyses of sample 09AL200 with $^{206}Pb/^{238}U$ ages ranging from 350 to 326 Ma yield a weighted mean age of 337 ± 5 Ma (MSWD = 2.0, 95% confidence interval), which is interpreted as the crystallization age of the South Diebusige monzogranites. Radiogenic Pb loss resulted in one analysis with a younger age than the main population (Fig. 5f).

In summary, based on the new zircon U–Pb age data, the granitoids in the South Diebusige, Diebusige, Bayanbulage and Hetun areas can be assigned to two epochs: Late Silurian (~423 Ma: the Bayanbulage quartz diorites) and Early Carboniferous (345–337 Ma: the Hetun, Diebusige and South Diebusige monzogranites).

4.2. Whole-rock major and trace element compositions

The Late Silurian quartz diorites from the Bayanbulage area have highly variable abundances of SiO_2, ranging from 58.0 to 67.9 wt.% (volatile free) (Fig. 6a). The Early Carboniferous monzogranites from the Hetun, Diebusige and South Diebusige areas show notably higher SiO_2 contents ranging from 71.5 to 76.7 wt.%. All of these rocks are low in TiO_2, $Fe_2O_3^T$, CaO, MgO ($Mg^{\#}$ (100 × [molar MgO / (MgO + FeO)]) = 27–46), K_2O and Na_2O contents (Table 1). On SiO_2 versus $K_2O + Na_2O$ and K_2O diagrams (Fig. 6a, b), they are plotted into the fields of subalkaline and high-K calcalkaline magmatic rocks, respectively. The Late Silurian quartz diorites have total $K_2O + Na_2O$ values ranging from 6.1 to 6.8 wt.% with low K_2O/Na_2O values of 0.75–0.81, but the Early Carboniferous monzogranites have higher total $K_2O + Na_2O$ values ranging from 7.0 to 8.5 wt.% with slightly higher K_2O/Na_2O values of 1.1–2.2. The quartz diorites and Early Carboniferous monzogranites have slightly variable A/CNK (molar $Al_2O_3/(CaO + Na_2O + K_2O)$) values of 0.82–1.07 and 1.02–1.15, respectively, and are plotted in the metaluminous to peraluminous and the weakly peraluminous fields, respectively (Fig. 6c).

The Late Silurian quartz diorites exhibit light rare earth element (LREE) enrichment and insignificant Eu anomalies on chondrite-normalized REE patterns (Fig. 7a). All of the Early Carboniferous granites, except sample 09AL127, have similar chondrite-normalized REE patterns with enrichment of LREE and insignificant Eu anomalies (Fig. 7c). On primitive mantle-normalized spidergrams, the granitoids show strong enrichment in Rb, Ba (except 09AL127), Th, Pb, and Sr, but pronounced negative anomalies in Nb, Ta, P and Ti relative to the neighbor elements (Fig. 7b, d). Sample 09AL127 has lower La to Gd, Sr, Ba, Zr and Th contents than other Hetun samples and a negative Eu anomaly, suggesting monazite + plagioclase + zircon fractionation in a highly silicic (73.36 wt.% SiO_2) granite. The negative anomalies in Nb, Ta, P and Ti (as well as the enrichment in Rb, Ba, Th, etc.) are not equivalent between the late Silurian quartz diorites and the Early Carboniferous granites and on average are more pronounced in the younger rocks.

The Early Carboniferous granites are geochemically characterized by relatively high Sr (≥252 ppm) but low Yb (≤1.3 ppm) and Y (≤11 ppm) contents with high Sr/Y ratios of 40–94 (except for two samples, 09AL127 and 09AL198, with low Sr/Y ratios of 9–28), similar to those of modern adakites and Archean tonalite–trondhjemite–granodiorite (TTG) suites (Fig. 8) (Defant and Drummond, 1990; Martin et al., 2005). In contrast, the Late Silurian quartz diorites show high Sr (333–704 ppm) and also high Yb (1.3–2.8 ppm) and Y (16–30 ppm) contents with low Sr/Y ratios of 21–24.

4.3. Whole rock Sr–Nd–Pb isotopic compositions

The whole rock Sr–Nd–Pb isotopic results are presented in Fig. 9. The Late Silurian quartz diorites exhibit variable initial $^{87}Sr/^{86}Sr$ isotopic ratios of 0.7073–0.7107 and have the highest $\varepsilon_{Nd}(t)$ values of −9.2 to −7.6 (Fig. 9a), corresponding to two-stage Nd mode ages (T_{2DM}) of

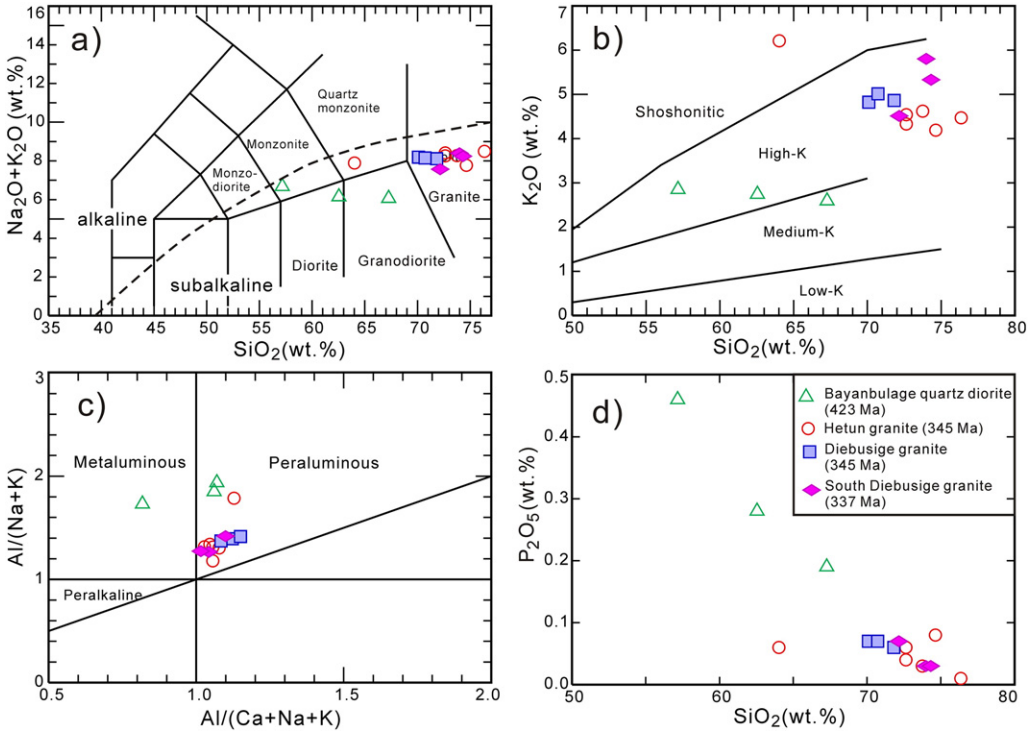

Fig. 6. (a) SiO_2 vs. $K_2O + Na_2O$ diagram for intrusive rocks (Middlemost, 1994); (b) SiO_2 vs. K_2O diagram (Peccerillo and Taylor, 1976); (c) plot of A/CNK vs. A/NK for the Paleozoic granitoids; (d) SiO_2 vs. P_2O_5 diagram.

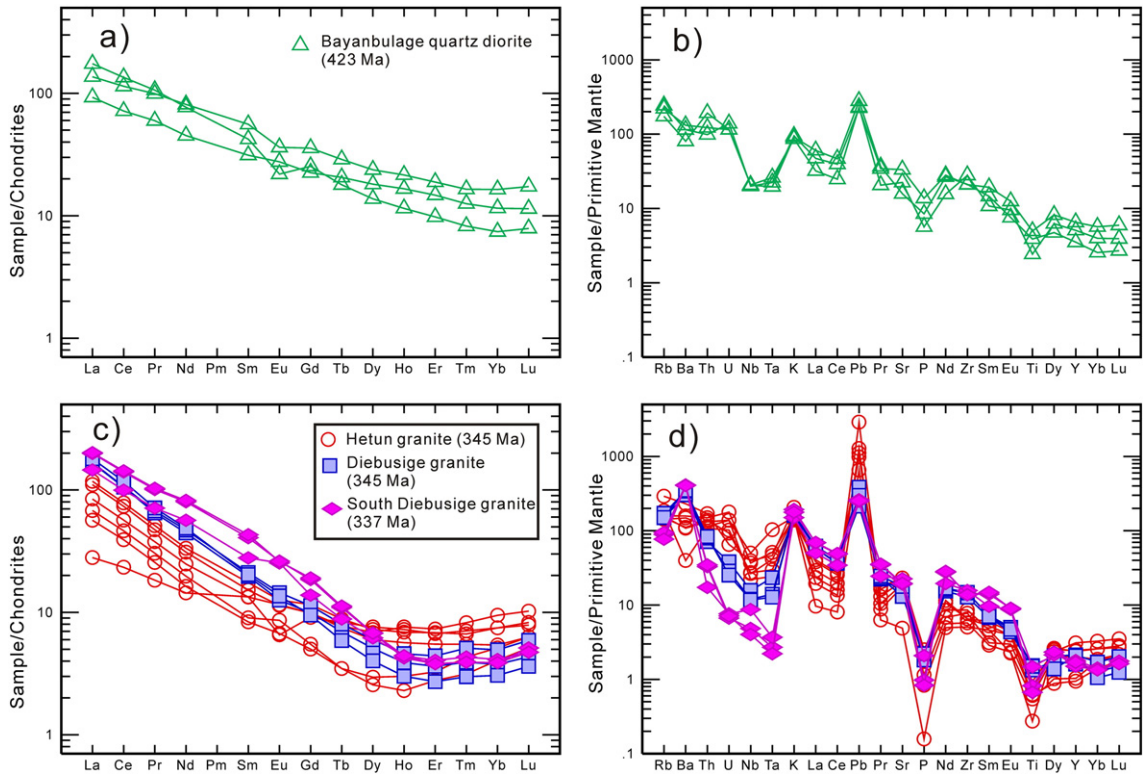

Fig. 7. Chondrite-normalized REE diagrams (a, c) and (b, d) primitive mantle-normalized incompatible trace element spidergrams for the Paleozoic granitoids. The normalization values are from Sun and McDonough (1989).

1.91–1.78 Ga. They exhibit radiogenic Pb isotope compositions ($^{206}Pb/^{204}Pb$ = 18.13–18.25, $^{207}Pb/^{204}Pb$ = 15.54–15.56 and $^{208}Pb/^{204}Pb$ = 38.35–38.45), which are plotted to the right of the 4.57 Ga Geochron (Fig. 9b). The Late Carboniferous granites from the Hetun area have lower initial $^{87}Sr/^{86}Sr$ isotopic ratios of 0.7043–0.7067 and $\varepsilon_{Nd}(t)$ values of −16.6 to −13.5, corresponding to two-stage Nd model ages of 2.42–2.20 Ga. The Hetun samples have intermediate Pb isotope compositions ($^{206}Pb/^{204}Pb$ = 17.25–18.22, $^{207}Pb/^{204}Pb$ = 15.41–15.51 and $^{208}Pb/^{204}Pb$ = 37.01–37.57), which straddle the 4.57 Ga Geochron (Fig. 9b). The Late Carboniferous granites from the Diebusige and South Diebusige areas have lower initial $^{87}Sr/^{86}Sr$ isotopic ratios of 0.7049–0.7060 and 0.7068–0.7070, and the lowest $\varepsilon_{Nd}(t)$ values of −19.2 to −19.0 and −18.1 to −18.0, corresponding to two-stage Nd mode ages (T_{2DM}) of 2.66–2.64 Ga and 2.57–2.56 Ga, respectively. They have unradiogenic Pb isotope compositions ($^{206}Pb/^{204}Pb$ = 16.06–16.36, $^{207}Pb/^{204}Pb$ = 15.28–15.32 and $^{208}Pb/^{204}Pb$ = 36.15–36.39), which are plotted to the left of the 4.57 Ga Geochron (Fig. 9b).

4.4. Zircon Hf–O isotopic compositions

Zircon Hf and oxygen isotope analyses were conducted on the same grains that were analyzed for U–Pb dating. The 423 Ma magmatic zircon grains from the Bayanbulage area sample 09AL147 have relatively homogeneous $\varepsilon_{Hf}(t)$ values of −8.6 to −5.3 (averaged at −6.8 ± 0.8 (1SD)), corresponding to two-stage zircon Hf model ages (T_{DM}^{C}) of 1.96–1.75 Ga (averaged at 1.84 ± 0.05 Ga (1SD)). By contrast, the 345–337 Ma magmatic zircon grains have a wide range of $\varepsilon_{Hf}(t)$ values.

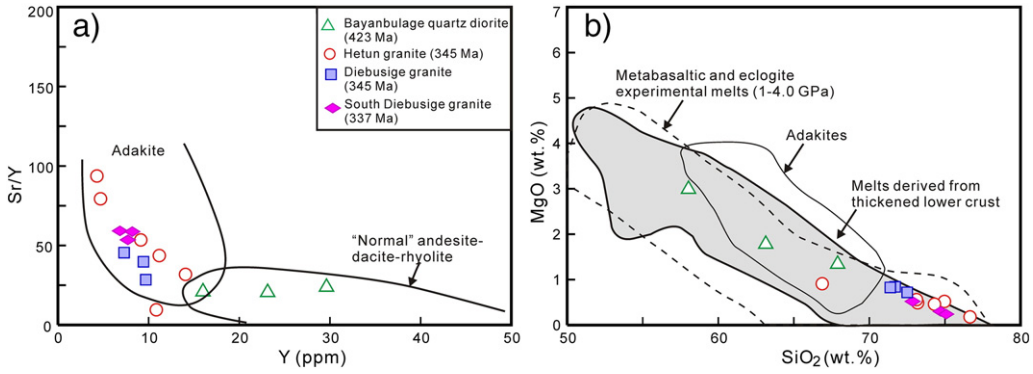

Fig. 8. (a) Sr/Y vs. Y diagram (after Defant et al., 2002); (b) SiO_2 vs. MgO diagram. The field of metabasaltic and eclogite experimental melts (1–4.0 GPa) is from the following references (Sen and Dunn, 1994; Rapp and Watson, 1995; Springer and Seck, 1997; Rapp et al., 1999; Skjerlie and Patiño Douce, 2002, and references therein). Fields of adakites inferred to be of subducting oceanic crust origin is after Q. Wang et al. (2006). Melts formed by partial melting of the lower mafic crust are from the following references (Atherton and Petford, 1993; Muir et al., 1995; Petford and Atherton, 1996; Johnson et al., 1997; Chung et al., 2003; Wang et al., 2005).

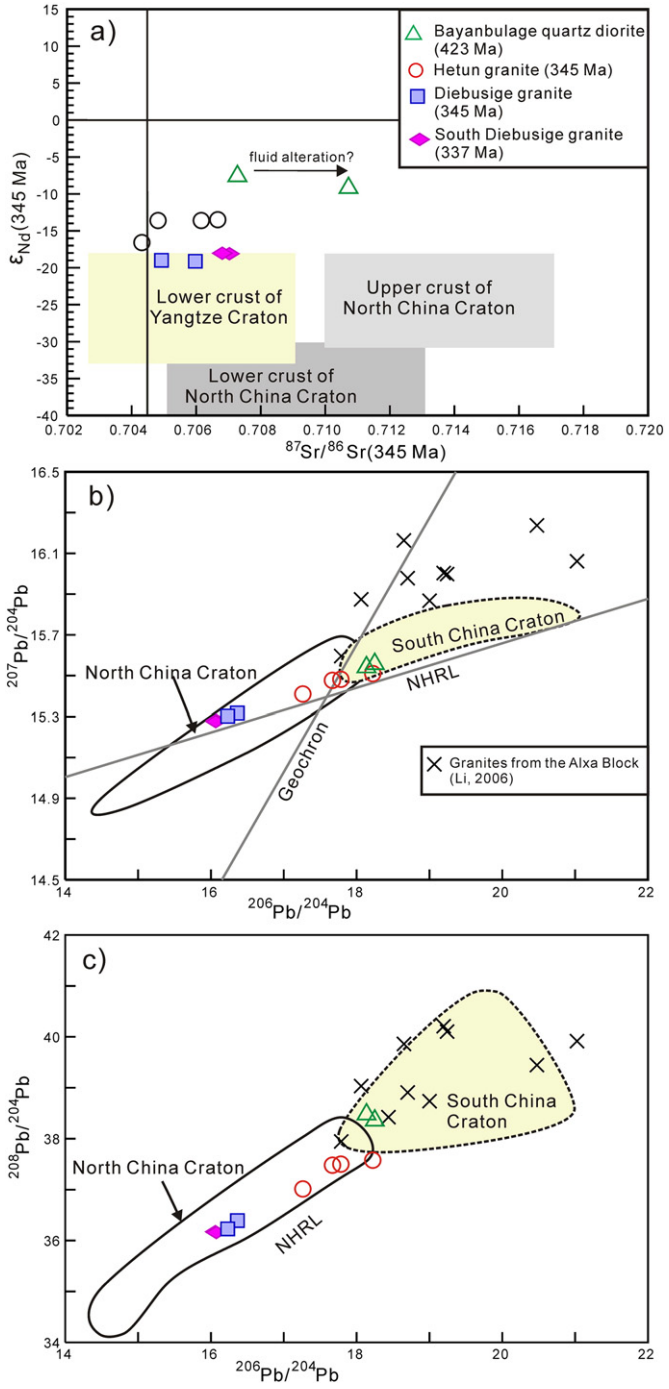

Fig. 9. (a) Nd–Sr isotopic compositions, (b) $^{206}Pb/^{204}Pb$ vs. $^{207}Pb/^{204}Pb$ and (c) $^{206}Pb/^{204}Pb$ vs. $^{208}Pb/^{204}Pb$ for the Paleozoic granitoids. The gray fields in (a) are from Jahn et al. (1999). Data sources for (b) and (c): the North China Craton (Liu et al., 2004; Li and Jiang, 2013 and references therein), the South China Craton (Zhang et al., 2000, 2007), NHRL (Hart, 1984).

The magmatic rocks from South Diebusige (sample 09AL200), Diebusige (09AL191 and 09AL198) and Hetun (09AL127 and 09AL131) have age-corrected $\varepsilon_{Hf}(t)$ values of −23.1 to −18.3, −18.5 to −13.0 and −14.6 to −7.4, corresponding to two-stage zircon Hf model ages of 2.79–2.50 Ga, 2.52–2.17 Ga and 2.28–1.82 Ga, respectively (Appendix 2).

The measured zircon $\delta^{18}O$ values from samples 09AL147, 09AL127, 09AL191, 09AL198 and 09AL200 show a limited range of 8.5–9.1‰, 5.7–6.9‰, 6.1–7.2‰, 5.9–6.7‰ and 6.1–7.2‰, forming normal Gaussian distributions, with respect to averages of 8.88 ± 0.17‰ (1SD), 6.32 ± 0.32‰ (1SD), 6.56 ± 0.27‰ (1SD), 6.34 ± 0.22‰ (1SD) and 6.49 ± 0.27‰ (1SD) (Fig. 10). The magmatic zircons from sample 09AL127, with slightly different ages, have similar $\delta^{18}O$ values (Appendix 2 and Fig. 10).

5. Discussion

5.1. The Alxa Block is not a part of the North China Craton

The Alxa Block has long been regarded as the westernmost part of the NCC (e.g., Kusky and Li, 2003; Zhao et al., 2005), with Archean basement rocks exposed on its eastern margin (NMBGMR, 1991). However, recent studies have revealed that only a few ~2.5 Ga TTG occur in the Alxa Block and these are located in the southwest (Gong et al., 2012; J.X. Zhang et al., 2013a). Moreover, ca. 930–910 Ma S-type granites were discovered in the Alxa Block, which were most likely formed in an orogenic compressional setting that is clearly distinct from the extensional tectonics associated with rift-related ca. 925–900 Ma mafic dykes in the central and eastern NCC (Dan et al., 2014a and references therein). Based on the discrepancy in the Precambrian geology between the Alxa Block and the NCC, we previously proposed that the Alxa Block is unlikely to be a part of the NCC (Dan et al., 2014a). This proposal is supported by the different detrital zircon age distributions in the Alxa Block and the NCC (Zhang et al., 2011; Dan et al., 2014a; Yuan and Yang, 2015a).

Our new Nd and Pb isotopic data also support the view that the Alxa Block is not a part of the NCC. The available Nd model ages of igneous rocks in the Bayanwulashan–Diebusige complexes are distinctly older than those of the Alxa Block, but are similar to those of the NCC (Fig. 13). The Pb isotopic compositions of Alxa Block magmatic rocks are more radiogenic than those of the North China Craton, but are akin to those of the South China Craton (Fig. 9b and C). Moreover, these new data suggest that the Bayanwulashan–Diebusige complexes are not a part of the Alxa Block as commonly suggested (e.g., Geng et al., 2010; Zhang et al., 2011; Dan et al., 2012; Li et al., 2012; Yuan and Yang, 2015a,b), and the western boundary of the NCC is likely located on the west fault of Bayanwulashan–Diebusige complexes (Fig. 2). The proposed boundary is also consistent with the deposition of similar Cambrian–Middle Ordovician carbonate rocks in the Helanshan and Bayanhot basins (Fig. 14) (Zhu et al., 1994; Wang, 2012), and the different sedimentary records in the Helanshan and Eastern Alxa Block (Fig. 14). It is notable that the Hetun monzogranites have younger crustal model ages (Fig. 13b) and intermediate Pb isotopic compositions (Fig. 9b, c), indicating that, in addition to a crustal component from the NCC, they may also contain an added crustal component from the Alxa Block.

5.2. Petrogenesis of the Paleozoic magmatism

5.2.1. The Silurian quartz diorites: Bayanbulage

Although a few Early Paleozoic igneous rocks have been reported in the eastern Alxa Block (Li, 2006), no detailed geochemical data were provided. We report the first zircon Hf–O isotopes for the Bayanbulage quartz diorites. The zircon grains have $\delta^{18}O$ values of 8.5–9.1‰, which are higher than most igneous zircon grains that typically have $\delta^{18}O$ values ranging from 5 to 8‰ (Valley et al., 2005; Cavosie et al., 2011). The notably high zircon $\delta^{18}O$ values imply involvement of ^{18}O-enriched supracrustal rocks in their generation, by either remelting and/or assimilation of such crustal rocks, or mixing between crust- and mantle-derived mafic magmas. The uniformity of $\varepsilon_{Nd}(t)$ values over large variations in SiO_2 contents for the quartz diorites (Table 2) indicates that crustal contamination is insignificant. The absence of xenocrystic zircons in sample 09AL147 also suggests that the effect of supracrustal contamination is insignificant. Unlike whole rocks, zircon grains have the capacity to record magma evolution processes (e.g., assimilation or mixing), which then result in large ranges in $\delta^{18}O$

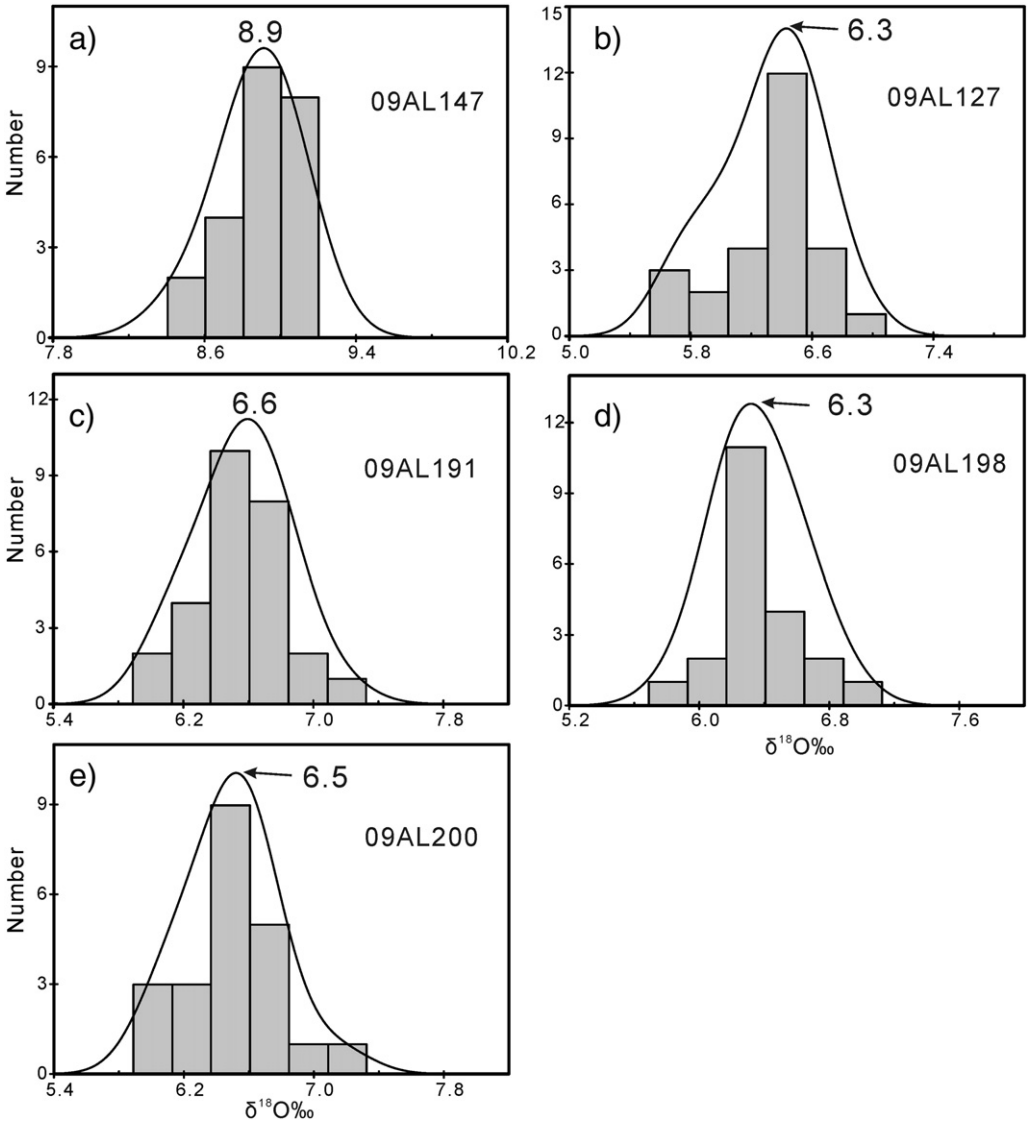

Fig. 10. Probability plots of zircon $\delta^{18}O$ values from the Paleozoic granitoids.

values and multiple peak values (e.g., Kemp et al., 2007; Appleby et al., 2008; Li et al., 2009; Dan et al., 2012). Thus, homogenous zircon $\delta^{18}O$ values suggest that their primary magmas were homogenous and did not suffer significant assimilation (e.g., Li et al., 2009; Dan et al., 2012). Although a magma mixing scenario is feasible if two different magmas have similar O isotope compositions, the unimodal distribution of zircon $\varepsilon_{Hf}(t)$ and the lack of correlation between Hf and O isotope compositions lend little support for magma mixing in this case. Thus, the crustal component implicated for these magmas was introduced at the site of magma generation, and the primary magma of the quartz diorites had high zircon ^{18}O values.

These high ^{18}O quartz diorites could have been generated by: (1) partial melting of the lower crust with high-$\delta^{18}O$ of 9.9‰ (Model 1) (e.g., Bindeman et al. 2004); and (2) addition of high-$\delta^{18}O$ (ca. 10–20‰) slab fluids into mantle-derived magma (e.g., Zi et al., 2012) (Model 2). Model 1 accounts for high $\delta^{18}O$ magmas by accretion of supracrustal materials to the pre-existing continental margin, followed by underthrusting of this material to a deep-crustal/upper-mantle location and mobilization via arc magmatism generated in a deep-crustal melting zone (Lackey et al., 2005; Roberts et al., 2013). Magmatic compositions generated by this mechanism range from gabbro to granite with a wide range of zircon $\delta^{18}O$ (5.4 to 8.7‰) and $\varepsilon_{Hf}(t)$ (+1 to +11) values (Roberts et al., 2013), in contrast to the homogeneous zircon O–Hf data of the single known quartz diorite from the Alxa Block. Differences between the predicted range of rock types and isotopic compositions and those identified in the Alxa Black clearly argue against Model 1. Although, Neoproterozoic S-type granites in the Alxa Block have high zircon $\delta^{18}O$ values (8.2–12.1‰) (Dan et al., 2014a), we note that they cannot be taken as the crustal end-member of the Model 1 mixed magma. Zircon Hf–O models indicate that an unrealistic 60–70% S-type granite contribution is required to produce the mixed magmas (Fig. 11). Thus, any potential crustal end member must have higher ^{18}O values than the S-type granites. In addition, the Bayanbulage quartz diorites might also be generated by partial melting of the former underplated basic magmatic rocks, which were produced by partial melting of SCLM (Model 2). Although this possibility could not be excluded, we do not prefer it because of their variable SiO_2 (58.0 to 67.9 wt.%) and Cr (27–59 ppm) and Ni (6.8–20 ppm) contents, which indicates significant crystal fractionation.

Although mantle metasomatism caused by high melt and fluid flux derived from subducted sediments and altered oceanic crust generally elevates $\delta^{18}O$ values up to ~2‰ (e.g., Bindeman et al. 2004; Martin et al. 2011), many examples demonstrate that magmas derived from

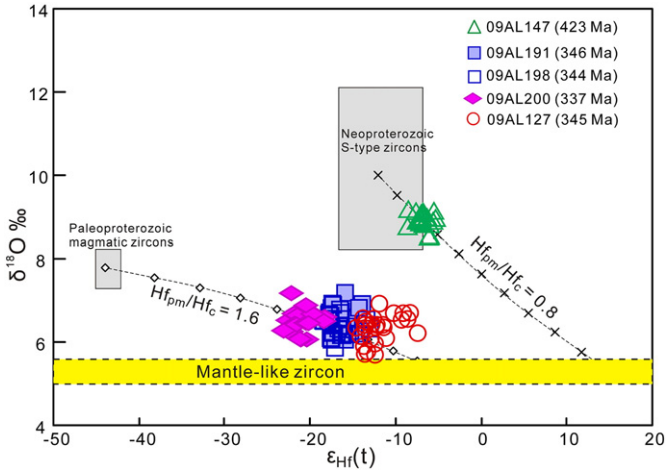

Fig. 11. Plot of zircon $\varepsilon_{Hf}(t)$ values vs. $\delta^{18}O$ values. The dashed lines denote the two-component mixing trends between the mantle- and supracrust-derived magmas. Hf_{pm}/Hf_c is the ratio of Hf concentration in the parental mantle magma (pm) over crustal (c) melt indicated for each curves, and the small rhombuses and ticks on the curves represent 10% mixing increments by arbitrary assuming that the mantle zircon has $\varepsilon_{Hf} = -5$ and $\delta^{18}O = 5.3‰$, and $\varepsilon_{Hf} = 15$ and $\delta^{18}O = 5.3‰$, respectively. The crust zircon for the 345 Ma rocks has $\varepsilon_{Hf} = -44$ and $\delta^{18}O = 7.8‰$, and supracrustal zircon for the 423 Ma rocks has $\varepsilon_{Hf} = -12$ and $\delta^{18}O = 10‰$. The magmatic zircon Hf–O values of the Paleoproterozoic rocks and Neoproterozoic S-type granites are from Dan et al. (2012, 2014a).

the sub-arc mantle can display significantly more ^{18}O-rich signatures ($\delta^{18}O$ value of 8.0–11.3‰) (Eiler et al., 1998, 2007; Liu et al., 2014). Partial melting of ^{18}O-enriched peridotites in the sub-arc mantle can generate mafic-intermediate rocks with high $\delta^{18}O$ values. One such diorite with a zircon $\delta^{18}O$ value of 8.7‰ was documented in the Sanjiang Orogen, SW China (Zi et al., 2012). The parent magmas of the Bayanbulage quartz diorites were likely generated by partial melting of subduction-modified subcontinental lithospheric mantle (SCLM). Their low $Mg^{\#}$ (36–45) and variable but low compatible trace element (e.g., Cr = 27–59 ppm and Ni = 6.8–20 ppm) indicate that their parent magmas underwent significant crystal fractionation.

5.2.2. The Early Carboniferous high Sr/Y monzogranites: Hetun, Diebusige and South Diebusige

As shown in Fig. 8, most of the Early Carboniferous monzogranites show some geochemical affinities with typical adakites as defined by

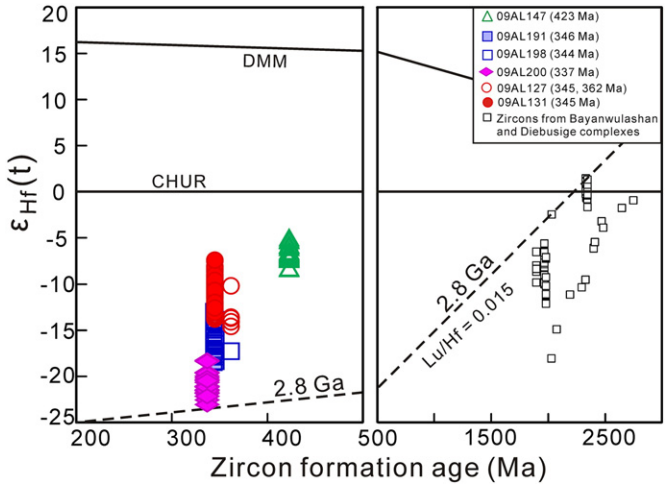

Fig. 12. Plot of $\varepsilon_{Hf}(t)$ values vs. crystallization ages for the zircons from the Paleoproterozoic (Dan et al., 2012) and Phanerozoic granitoids, illustrating that the Phanerozoic granitoids are not generated by directing partial melting of the Paleoproterozoic rocks.

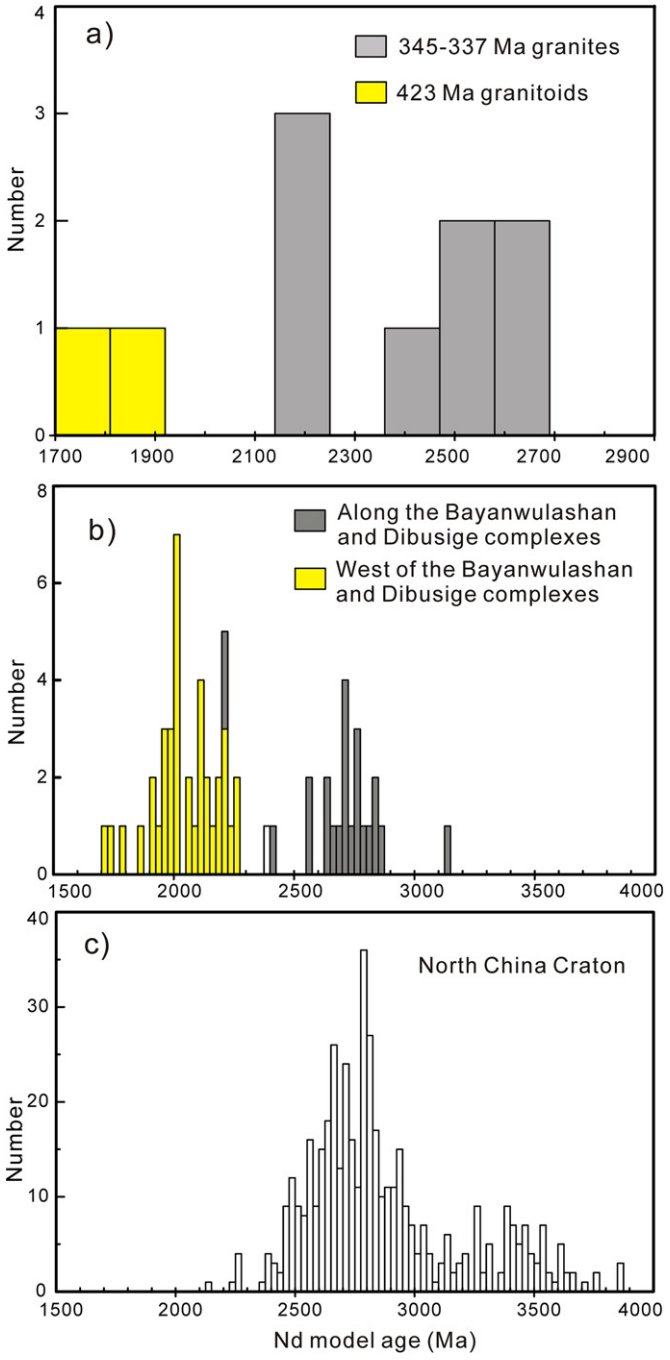

Fig. 13. Whole rock Nd model ages for (a) the 423–337 Ma granitoids, (b) the Paleoproterozoic–Permian rocks (Sources: Dan, 2011; Dan et al., 2014a,b and this study) in eastern Alxa Block, and (c) Archean–Paleoproterozoic rocks in the North China Craton (data compiled by Wu et al., 2005).

Defant and Drummond (1990). However, their high K_2O contents (Table 1) and K_2O/Na_2O ratios (1.1–2.2) are inconsistent with typical adakitic rocks, but similar to high Sr/Y granites (Moyen, 2009). In addition, the presence of a significant negative Eu anomaly and low Sr content (103 ppm) in Hetun monzogranite sample 09AL127 indicate that plagioclase fractionation likely played an important role in their generation. This is also inconsistent with the characteristics of adakitic rocks.

Several models have been proposed for the generation of high Sr/Y granitoids, including (a) melting of subducted young and hot oceanic crust (e.g., Defant and Drummond, 1990; Kay et al., 1993; Martin et al., 2005; Wang et al., 2007a, 2008a); (b) assimilation and fractional crystallization (AFC) or fractional crystallization (FC) from parental

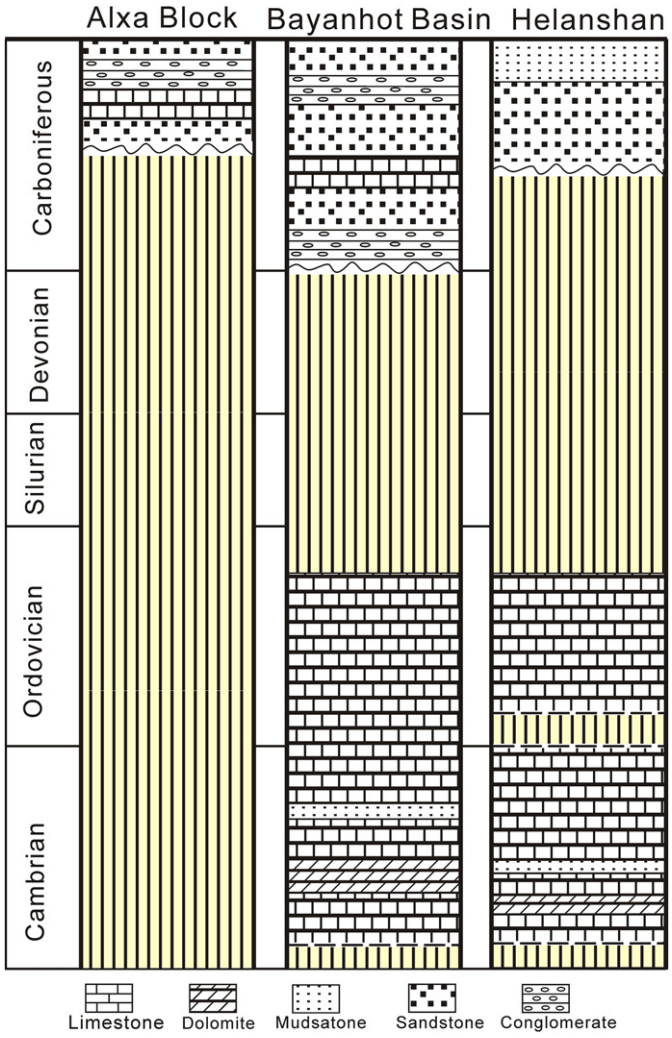

Fig. 14. Correlation diagram of the Paleozoic strata in the northwest North China (data based on NMBGMR, 1991; Li, 2006; Zhang et al., 2011; Wang, 2012).

basaltic magmas (Castillo et al., 1999; Macpherson et al., 2006; Richards and Kerrich, 2007; Rooney et al., 2011); (c) magma mixing between felsic and basaltic magmas (Guo et al., 2007; Streck et al., 2007); and (d) partial melting of thickened lower crust (Atherton and Petford, 1993; Petford and Atherton, 1996; Chung et al., 2003; Wang et al., 2005). In the case of the Early Carboniferous monzogranites, the first three models cannot account for the petrogenesis of these rocks. Oceanic slab melting is unlikely to have generated these high Sr/Y granitoids because of the apparent lack of contemporaneous subduction in the eastern Alxa Block, their high K_2O/Na_2O ratios and their evolved Sr–Nd–Hf isotopic compositions (Figs. 9 and 12). Magmatic rocks generated by fractional crystallization processes generally exhibit a continuous compositional trend from basaltic rocks derived from mantle to felsic rocks derived from residual magmas (e.g., Castillo et al., 1999; Macpherson et al., 2006; Richards and Kerrich, 2007). Although minor fractional crystallization may be involved in the genesis of these Early Carboniferous high Sr/Y rocks, the absence of contemporary basaltic and intermediate igneous rocks associated with these granitoids rules out a significant role for this process. Similar rocks formed by magma mixing usually display intermediate compositions combined with high Mg (e.g., adakitic high-Mg andesites) (Guo et al., 2007; Streck et al., 2007) rather than the acidic adakitic rocks identified in the present study area. Based on the absence of contemporary basaltic rocks and the homogeneity of magma revealed by O and Hf isotopes, magma mixing is also unlikely to have been a dominant process in the generation of such high Sr/Y granitoids. Consequently, the remaining possibility of partial melting of thickened lower crust is considered in detail below.

Partial melting of a thickened garnet-bearing mafic lower crust due to heat flux from the mantle (e.g., Atherton and Petford, 1993; Wang et al., 2005; X.C. Wang et al., 2006; Wang et al., 2007b) appears to be a plausible mechanism for the generation of the Carboniferous high Sr/Y rocks near the eastern Alxa Block. For example, the model predicts low compatible element contents (e.g., MgO, Cr, Ni and Co). In Fig. 8b, the samples display linear trends that are parallel to the fields of melts formed by partial melting of the thickened lower crust, a scenario that is supported by the contemporaneous westward ductile thrusting in this area (J. Zhang et al., 2013a). It is also consistent with the relatively low zircon $\delta^{18}O$ values (6.3–6.6‰) (Fig. 10), which are below or only slightly higher than the published upper limit value of mantle-derived magma (6.5‰) (e.g., Valley et al., 2005). In addition, the Hetun monzogranites are characterized by concave REE patterns (Fig. 7c), which are indicative of hornblende fractional crystallization or the presence of hornblende in the residual mineral assemblage.

The Carboniferous high Sr/Y rocks have negative $\varepsilon_{Nd}(t)$ (−19.2 to −13.5) and old Nd model ages (2.66–2.20 Ga), suggesting that they originated from old (Archean or Paleoproterozoic) crustal rocks. It is notable that the model ages of the high Sr/Y rocks are younger than the values of the Bayanwulashan and Diebusige complexes. The Hetun monzogranites have Nd model ages of 2.42–2.20 Ga that are distinctly lower than the 2.85–2.65 Ga (Dan, 2011) model ages of the Paleoproterozoic Bayanwulashan Complex. The 345–337 Ma high Sr/Y rocks from Diebusige and South Diebusige have Nd model ages of 2.66–2.56 Ga, which are lower than the 3.14–2.79 Ga age of the Diebusige Complex (Dan, 2011). These results imply that these 345–337 Ma high Sr/Y rocks were not directly derived from the Bayanwulashan and Diebusige complexes (Fig. 12). Moreover, the zircon $\delta^{18}O$ values of the high Sr/Y rocks (6.3–6.6‰) are lower than those (7.3–8.2‰) of mafic and felsic rocks from the Bayanwulashan and Diebusige complexes (Dan et al., 2012 and our unpublished data). Therefore, we suggest that the high Sr/Y rocks were likely generated by partial melting of basaltic lower crust that was underplated after the formation of the Paleoproterozoic Bayanwulashan and Diebusige complexes. The zircon Hf–O isotopic compositions suggest that the proportion of mantle-derived magmas involved in generating the high Sr/Y rocks could have been as high as 75% (Fig. 11). We note that the mafic end-members were probably more radiogenic, thus, the calculated proportions of mantle components involved in the granite formation are the minimum estimates.

5.3. A cryptic suture zone between the Alxa Block and North China Craton

In view of the different evolutionary histories of the Alxa Block and the NCC during the Neoproterozoic, a Phanerozoic orogenic belt or suture zone, which resulted in their amalgamation, has recently been inferred (Dan et al., 2014a). In previous studies, most researchers suggest that the suture zone between the Alxa Block and NCC is the western fault of Helanshan (Zhang et al., 2011; Li et al., 2012; Yuan and Yang, 2015a,b) based on the strong deformation of the strata in the Helanshan Basin and adjacent area. However, there are almost no Paleozoic magmatism, metamorphism and ophiolites discovered along this suture zone. Moreover, the Bayanhot and Helanshan basins were considered as foreland basins formed during the collision between the Alxa and the Qilian blocks (Xiong et al., 2001; Zhang et al., 2011). However, both of them lack Silurian–Devonian strata (Yuan and Geng, 1992; Xiong et al., 2001; Zhang et al., 2011; Wang, 2012), which contrast with the contemporaneous thick flysch strata in the Hexi Corridor foreland basin formed during the collision between the Alxa and Qilian blocks (e.g., Du et al., 2004). The NE trending of these basins is also different with the NW trending of the Hexi Corridor foreland basin. Thus, all these scenarios argue against this conventional suture zone, and a

new proposed suture zone should explain the formation of the Bayanhot and Helanshan basins.

As stated above, the scarcity of documented Paleozoic magmatic and metamorphic events in the eastern Alxa Block has hindered attempts to delineate the relationship between the Alxa Block and the NCC. The newly-identified Silurian to Early Carboniferous igneous rocks, combined with previous reported Early Paleozoic igneous ages (Li, 2006), provide a basis for assessing the possible nature of a Phanerozoic suture zone and the timing of Alxa Block–North China Craton amalgamation.

Most of the Phanerozoic igneous rocks exposed in the Alxa Block were formed between 320 Ma and 260 Ma (see a review in Dan et al., 2014b) with scarce Early Paleozoic to Early Carboniferous igneous rocks only reported on the eastern margin of the Alxa Block and adjacent areas (Fig. 2). In addition to the studied Late Silurian quartz diorites (~423 Ma) and the Early Carboniferous monzogranites (345–337 Ma), Li (2006) reported ~394 Ma diorites in the Bayanwulashan Complex and ~447 Ma andesites–dacites–rhyolites and granodiorites in the eastern Alxa Block using zircon U–Pb TIMS dating. Many detrital zircon grains with an age population of 482–401 Ma were also reported in the Upper Paleozoic strata (Li, 2006; Chen et al., 2010). Thus, a linear zone of Early Paleozoic to Early Carboniferous granitoids (Fig. 2) is identified in the eastern Alxa Block. These igneous rocks can be divided into Early Paleozoic (447?–423 Ma) and Late Paleozoic (345–337 Ma) stages. The Late Paleozoic high Sr/Y granites, generated by partial melting of thickened lower crust, were likely produced in an orogen (e.g., Chung et al., 2003; Wang et al., 2005, 2007b, 2008b; Karsli et al., 2010; He et al., 2011) or a cryptic suture zone (Su et al., 2013).

The Early Paleozoic igneous rocks consist of andesites–dacites–rhyolites, granodiorites and quartz diorites, however, only the Late Silurian quartz diorites have geochemical data available to constrain their tectonic setting. I-type granitoids can be generated in continental rift settings but these environments commonly also contain abundant basalt (e.g., Li et al., 2003). In the Alxa Block, however, there are no contemporaneous basalts or other large volume igneous rocks, which argues against a continental rift setting. Notably, the Early Paleozoic rocks have high zircon $\delta^{18}O$ values (8.5–9.1‰), indicating that they were either sourced from subducted low-temperature hydrothermally altered igneous rocks or their sources were metasomatised by subducted sedimentary rocks. These scenarios commonly occur at convergent continental margins (Lackey et al., 2005; Zi et al., 2012) or along terrane boundaries (Peck et al., 2004). Thus, the quartz diorites were most likely produced at a continental boundary, although the tectonic settings of active continental margin or collisional orogen cannot be distinguished based on available geochemical data.

The proposed cryptic suture zone can perfectly explain the lack Silurian–Devonian strata and the NE trending of the Bayanhot and Helanshan basins. We accepted that the Bayanhot Basin and the adjacent Helanshan Basin were foreland basins (Xiong et al., 2001; Zhang et al., 2011), but they were not formed during the collision between the Qilian and the Alxa blocks. Taking into account the NE-trending of the Bayanhot and Helanshan basins, they probably constitute a foreland basin system formed during the collision between the Alxa Block and the NCC. Thus, the united Alxa Block–North China Craton could lack Silurian–Devonian strata, different from the contemporaneous thick flysch strata in the Hexi Corridor foreland basin formed during the collision between the Alxa and Qilian blocks (e.g., Du et al., 2004). The foreland basin system commonly records the evolution of the adjacent orogen (e.g., Li et al., 1999; Decelles, 2012; Wu et al., 2014). Thus, the timing of the amalgamation of the Alxa Block and North China Craton may be approximately constrained by the unconformity between the Early Paleozoic and Late Paleozoic strata in the Bayanhot Basin and adjacent area located in the westernmost part of the NCC (Fig. 14). The pre-Middle Ordovician strata underwent strong deformation evidenced by congruent folds with axial planes striking N–S, along with the less deformed Devonian–Carboniferous strata (Li et al., 2012), further suggesting that a collisional event took place before the Devonian period (Li et al., 2012).

Recently, metamorphic age of 399 ± 6 Ma (LA-ICP-MS zircon U–Pb) was obtained from a garnet-bearing amphibolite in the Baoyintu Group in the northern proposed suture zone (Chen et al., 2014). Based on the clockwise P–T path, this age was interpreted as the collision age between the CAOB and the NCC (Chen et al., 2014). However, the studied Baoyintu Group is NE trending, and is a part of the proposed orogen between the Alxa Block and the NCC. Moreover, the Baoyintu Group underwent strong deformation and formed anticline with axial direction of NE. Thus, the metamorphism age of 399 Ma is likely approximate to the collision age between the Alxa Block and the NCC.

In previous studies, many approaches have been applied to determine the precise collision time between the Alxa Block and the NCC. Based on the palaeomagnetic data, the timing is suggested to be in Late Cambrian (Huang et al., 1999, 2000) or Triassic (Yuan and Yang, 2015b). As pointed by J. Zhang et al. (2013b), an Early Permian orogenic granitoid belt and Triassic anorogenic alkaline rock belt occurred in the Northern North China Craton and Alxa Block, indicating that the amalgamation of the Alxa Block and NCC probably was prior to Early Permian. Recently, J. Zhang et al. (2013a) discovered the westward ductile thrusting on the western margin fault of Bayanwulashan, which probably occurred at ca. 345 Ma, contemporaneous with the production of the Late Paleozoic high Sr/Y granites (345–337 Ma). This stage of westward ductile thrusting was inferred to have resulted from the collision between the Alxa Block and North China Craton (J. Zhang et al., 2013a). However, the collision time obtained by these approaches is commonly less than the initial collision time between two blocks (Li et al., 1999; Wu et al., 2014).

After the initial collision, the rocks of the active continental margin are typically uplifted, eroded and transported into the foreland basin on the opposing passive margin (Decelles, 2012; Wu et al., 2014). Therefore, the appearance of the Alxa-derived detritus on the NCC continental margin should provide direct evidence of this collision. The detrital zircons from the Paleozoic strata exposed between the Bayanhot Basin and the western fault of Helanshan can be used to infer the materials derived from the Alxa Block. There are no Paleozoic zircons in Cambrian strata but in Late Ordovician (youngest age peak is 450 Ma) (Zhang et al., 2011, 2012), indicating that the initial collision between the Alxa Block and the NCC possibly occurred in Late Ordovician.

In summary, the inferred suture zone is supported by the linear distribution of the Early Paleozoic–Early Carboniferous granitoids, the high zircon $\delta^{18}O$ value of the Late Silurian quartz diorites, and the foreland basin system formed during the collision between the Alxa Block and the NCC. The timing of collision can be constrained by the unconformity of Early Paleozoic and Late Paleozoic strata and the strong deformation of the Early Paleozoic strata in the westernmost NCC, and the 399 Ma amphibolite-facies metamorphism in the Lanshan belt. The detrital zircon data further suggest that the Alxa-derived clastic sediments have contributions to sedimentation on the NCC continental margin in Late Ordovician.

6. Conclusions

We draw the following conclusions based on our new geochronological and geochemical data:

(1) High-precision SIMS U–Pb zircon dating indicates that the Bayanbulage quartz diorites crystallized at ca. 423 Ma, and the Hetun, Diebusige and South Diebusige monzogranites at ca. 345–337 Ma. The Late Silurian (ca. 423 Ma) quartz diorites were formed by partial melting of old crust of normal thickness whereas the Early Carboniferous (ca. 345–337 Ma) high Sr/Y monzogranites were generated by remelting of thickened lower crust.

(2) The Nd model ages and Pb isotope compositions are distinct on either side of the fault bounding the western margins of the Bayanwulashan–Diebusige complexes, suggesting that the Alxa Block is not a part of the North China Craton, and the western boundary of the North China Craton is located on the west fault of the Bayanwulashan–Diebusige complexes.
(3) Available data, including the linear distribution of the Late Silurian–Early Carboniferous granitoids in eastern Alxa Block, the high zircon $\delta^{18}O$ value of the Late Silurian quartz diorites, the Early Devonian metamorphism and the foreland basin system occurring during the collision between the Alxa Block and the NCC, indicate the potential existence of a suture zone in the vicinity of the eastern Alxa Block, resulting from the amalgamation of the Alxa Block and North China Craton. The timing of initial collision may be in Late Ordovician.
(4) If the proposed revision to the tectonic history of the Alxa Block and North China Craton proposed here is supported by further studies, then the present models of the Craton's relationship to the Columbia supercontinent will require revision.

Supplementary data to this article can be found online at http://dx.doi.org/10.1016/j.gr.2015.02.011.

Acknowledgments

We thank Q. L. Li and G. Q. Tang for their help in SIMS analyses and Y. H. Yang for LA-MC-ICP-MS analyses. Thoughtful and constructive comments by Professor W.J. Xiao and two anonymous reviewers substantially improved the manuscript. This study was financially supported by Strategic Priority Research Program (B) of the Chinese Academy of Sciences (Grant No. XDB03010600), the Major State Basic Research Program (973 Program) of the People's Republic of China (Grant No. 2011CB808906), State Key Laboratory of Lithospheric Evolution, IGGCAS , National Natural Science Foundation of China (Grant Nos. 41025006 and 41303018) and the Guangzhou Institute of Geochemistry, Chinese Academy of Sciences (GIGCAS 135 project Y234021001). This is contribution No. IS-2047 from GIGCAS, and TIGeR (The Institute of Geoscience Research) Publication No. 613.

References

Andersen, T., 2002. Correction of common lead in U–Pb analyses that do not report ^{204}Pb. Chemical Geology 192, 59–79.
Appleby, S.K., Graham, C.M., Gillespie, M.R., Hinton, R.W., Oliver, G.J.H., EIMF, 2008. A cryptic record of magma mixing in diorites revealed by high-precision SIMS oxygen isotope analysis of zircons. Earth and Planetary Science Letters 269, 105–117.
Atherton, M.P., Petford, N., 1993. Generation of sodium-rich magmas from newly underplated basaltic crust. Nature 362, 144–146.
Belousova, E.A., Griffin, W.L., O'Reilly, S.Y., Fisher, N.I., 2002. Igneous zircon: trace element composition as an indicator of source rock type. Contributions to Mineralogy and Petrology 143, 602–622.
Bindeman, I.N., Ponomareva, V.V., Bailey, J.C., Valley, J.W., 2004. Volcanic arc of Kamchatka: a province with high-$\delta^{18}O$ magma sources and large-scale $^{18}O/^{16}O$ depletion of the upper crust. Geochimica et Cosmochimica Acta 68, 841–865.
Bleeker, W., 2003. The late Archean record: a puzzle in ca. 35 pieces. Lithos 71, 99–134.
Castillo, P.R., Janney, P.E., Solidum, R.U., 1999. Petrology and geochemistry of Camiguin Island, southern Philippines: insights to the source of adakites and other lavas in a complex arc setting. Contributions to Mineralogy and Petrology 134, 33–51.
Cavosie, A.J., Valley, J.W., Kita, N.T., Spicuzza, M.J., Ushikubo, T., Wilde, S.A., 2011. The origin of high $\delta^{18}O$ zircons: marbles, megacrysts, and metamorphism. Contributions to Mineralogy and Petrology 162, 961–974.
Chen, D.C., Zhao, X.M., Deng, J., 2010. Redefinition of Upper Triassic strata on the northern margin of Alxa Block; constraints from laser ICP-MS detrital zircon U–Pb ages. Acta Petrologica et Mineralogica 29, 258–270.
Chen, Y.P., Wei, C.J., Zhang, J.R., Chu, H., 2014. Metamorphism and geochronology for the Baoyintu Group in middle-western Inner Mongolia. Annual Meeting of Chinese Geoscienc Union (CGU), Abstracts. 2152 (in Chinese).
Chung, S.L., Liu, D.Y., Ji, J.Q., Chu, M.F., Lee, H.Y., Wen, D.J., Lo, C.H., Lee, T.Y., Qian, Q., Zhang, Q., 2003. Adakites from continental collision zones: melting of thickened lower crust beneath southern Tibet. Geology 31, 1021–1024.
Dan, W., 2011. Precambrian Evolution of the Westernmost North China Craton: Geochronological and Geochemical Constraints. (Ph.D. thesis), Institute of Geology and Geophysics, China Academy of Sciences, Beijing (143 pp.).
Dan, W., Li, X.H., Guo, J.H., Liu, Y., Wang, X.C., 2012. Paleoproterozoic evolution of the eastern Alxa Block, westernmost North China: evidence from in situ zircon U–Pb dating and Hf–O isotopes. Gondwana Research 21, 838–864.
Dan, W., Li, X.H., Wang, Q., Wang, X.C., Liu, Y., 2014a. Neoproterozoic S-type granites in the Alxa Block, westernmost north China and tectonic implications: in-situ zircon U–Pb–Hf–O isotopic and geochemical constraints. American Journal of Sciences 314, 110–153.
Dan, W., Li, X.H., Wang, Q., Tang, G.J., Liu, Y., 2014b. The Early Permian (ca. 280 Ma) silicic igneous province in Alxa Block, NW China: a magmatic flare-up triggered by a mantle-plume? Lithos 204, 144–158.
Decelles, P.G., 2012. Chapter 20, Foreland basin systems revisited: variations in response to tectonic settings. In: Busby, C., Azor Pérez, A. (Eds.), Tectonics of Sedimentary Basins: Recent Advances, First edition Blackwell Publishing Ltd., pp. 405–426.
Defant, M.J., Drummond, M.S., 1990. Derivation of some modern arc magmas by melting of young subducted lithosphere. Nature 347, 662–665.
Defant, M.J., Xu, J.F., Kepezhinskas, P., Wang, Q., Zhang, Q., Xiao, L., 2002. Adakites: some variations on a theme. Acta Petrologica Sinica 18, 129–142.
Dong, C.Y., Liu, D.Y., Li, J.J., Wan, Y.S., Zhou, H.Y., Li, C.D., Yang, Y.H., Xie, L.W., 2007. Palaeoproterozoic Khondalite Belt in the western North China Craton: new evidence from SHRIMP dating and Hf isotope composition of zircons from metamorphic rocks in the Bayan Ul–Helan Mountains area. Chinese Science Bulletin 52, 2984–2994 (in Chinese with English abstract).
Du, Y.S., Zhu, J., Han, X., Gu, S.Z., 2004. From the back-arc basin to foreland basin—Ordovician–Devonian sedimentary basin and tectonic evolution in the North Qilian orogenic belt. Geological Bulletin of China 23, 911–917 (in Chinese with English abstract).
Eiler, J.M., McInnes, B., Valley, J.W., Graham, C.M., Stolper, E.M., 1998. Oxygen isotope evidence for slab-derived fluids in the sub-arc mantle. Nature 393, 777–781.
Eiler, J.M., Schiano, P., Valley, J.W., Kita, N.T., Stolper, E.M., 2007. Oxygen-isotope and trace element constraints on the origins of silica-rich melts in the subarc mantle. Geochemistry, Geophysics, Geosystems 8, Q09012. http://dx.doi.org/10.1029/2006GC001503.
Geng, Y.S., Wang, X.S., Wu, C.M., Zhou, X.W., 2010. Late-Paleoproterozoic tectonothermal events of the metamorphic basement in Alxa area: evidence from geochronology. Acta Petrologica Sinica 26, 1159–1170 (in Chinese with English abstract).
Gong, J.H., Zhang, J.X., Yu, S.Y., Li, H.K., Hao, K.J., 2012. The ~2.5 Ga TTG in the western Alxa Block and its geological significance. Science China Bulletin 57, 2715–2728.
Guo, F., Nakamuru, E., Fan, W.M., Kobayoshi, K., Li, C.W., 2007. Generation of Palaeocene adakitic andesites by magma mixing, Yanji Area, NE China. Journal of Petrology 48, 661–692.
Hart, S.R., 1984. A large-scale isotope anomaly in the southern hemisphere mantle. Nature 309, 753–757.
He, Y., Li, S., Hoefs, J., Huang, F., Liu, S.A., Hou, Z., 2011. Post-collisional granitoids from the Dabie orogen: new evidence for partial melting of a thickened continental crust. Geochimica et Cosmochimica Acta 75, 3815–3838.
Hou, G., Santosh, M., Qian, X., Lister, G.S., Li, J., 2008. Configuration of the Late Paleoproterozoic supercontinent Columbia: insights from radiating mafic dyke swarms. Gondwana Research 14, 395–409.
Huang, B.C., Yang, Z.Y., Otofuji, Y.I., Zhu, R.X., 1999. Early Paleozoic paleomagnetic poles from the western part of the North China Block and their implications. Tectonophysics 308, 377–402.
Huang, B.C., Otofuji, Y.I., Yang, Z.Y., Zhu, R.X., 2000. Preliminary result and its tectonic implications of Middle Cambrian paleomagnetism in the Alashan and Hexi Corridor terrane. Chinese Journal of Geophysics 43, 393–401 (in Chinese with English abstract).
Jackson, S.E., Pearson, N.J., Griffin, W.L., Belousova, E.A., 2004. The application of laser ablation-inductively coupled plasma-mass spectrometry to in situ U–Pb zircon geochronology. Chemical Geology 211, 47–69.
Jahn, B.M., Wu, F.Y., Lo, C.H., Tsai, C.H., 1999. Crust–mantle interaction induced by deep subduction of the continental crust: geochemical and Sr–Nd isotopic evidence from post-collisional mafic–ultramafic intrusions of the northern Dabie complex, central China. Chemical Geology 157, 119–146.
Johnson, K., Barnes, C.G., Miller, C.A., 1997. Petrology, geochemistry, and genesis of high-Al tonalite and trondhjemites of the Cornucopia Stock, Blue Mountains, Northeastern Oregon. Journal of Petrology 38, 1585–1611.
Karsli, O., Dokuz, A., Uysal, İ., Aydin, F., Kandemir, R., Wijbrans, J., 2010. Generation of the Early Cenozoic adakitic volcanism by partial melting of mafic lower crust, Eastern Turkey: implications for crustal thickening to delamination. Lithos 114, 109–120.
Kay, S.M., Ramos, V.A., Marquez, M., 1993. Evidence in Cerro Pampa volcanic rocks of slab melting prior to ridge trench collision in southern South America. The Journal of Geology 101, 703–714.
Kemp, A.I., Hawkesworth, C.J., Foster, G.L., Paterson, B.A., Woodhead, J.D., Hergt, J.M., Gray, C.M., Whitehouse, M.J., 2007. Magmatic and crustal differentiation history of granitic rocks from Hf–O isotopes in zircon. Science 315, 980–983.
Kusky, T.M., Li, J.H., 2003. Paleoproterozoic tectonic evolution of the North China Craton. Journal of Asian Earth Sciences 22, 383–397.
Kusky, T.M., Santosh, M., 2009. The Columbia connection in North China. Geological Society of London, Special Publication 323, 49–71.
Kusky, T.M., Li, J.H., Santosh, M., 2007. The Paleoproterozoic North Hebei Orogen: North China Craton's collisional suture with the Columbia supercontinent. Gondwana Research 12, 4–28.
Lackey, J., Valley, J., Saleeby, J., 2005. Supracrustal input to magmas in the deep crust of Sierra Nevada batholith: evidence from high-O zircon. Earth and Planetary Science Letters 235, 315–330.

Li, J.J., 2006. Regional Metallogenic system of Alashan Block in Inner Monolia Automomous Region. (Ph.D. thesis), China University of Geosciences, Beijing (177 pp.).
Li, T.J., Jiang, N., 2013. Links between Mesozoic intermediate-felsic igneous rocks and lower crustal granulite xenoliths, North China Craton: O and Pb isotopic evidence. International Geology Review 55, 442–452.
Li, J.L., Su, S., Hao, J., Chen, H.H., Hou, Q.L., Xiao, W.J., Wu, J.M., 1999. Time limit of collision event of collision orogens. Acta Petrologica Sinica 15, 315–320 (in Chinese with English abstract).
Li, X.H., Sun, M., Wei, G.J., Liu, Y., Lee, C.Y., Malpas, J., 2000. Geochemical and Sm–Nd isotopic study of amphibolites in the Cathaysia Block, southeastern China: evidence for an extremely depleted mantle in the Paleoproterozoic. Precambrian Research 102, 251–262.
Li, X.H., Li, Z.X., Ge, W., Zhou, H., Li, W., Liu, Y., Wingate, M.T.D., 2003. Neoproterozoic granitoids in South China: crustal melting above a mantle plume at ca. 825 Ma? Precambrian Research 122, 45–83.
Li, X.H., Liu, D.Y., Sun, M., Li, W.X., Liang, X.R., Liu, Y., 2004. Precise Sm–Nd and U–Pb isotopic dating of the supergiant Shizhuyuan polymetallic deposit and its host granite, SE China. Geological Magazine 141, 225–231.
Li, X.H., Qi, C.S., Liu, Y., Liang, X.R., Tu, X.L., Xie, L.W., Yang, Y.H., 2005. Petrogenesis of the Neoproterozoic bimodal volcanic rocks along the western margin of the Yangtze Block: new constraints from Hf isotopes and Fe/Mn ratios. Chinese Science Bulletin 50, 2481–2486.
Li, X., Li, W., Wang, X., Li, Q., Liu, Y., Tang, G., 2009. Role of mantle-derived magma in genesis of early Yanshanian granites in the Nanling Range, South China: in situ zircon Hf–O isotopic constraints. Science in China Series D: Earth Sciences 52, 1262–1278.
Li, X.H., Li, W.X., Li, Q.L., Wang, X.C., Liu, Y., Yang, Y.H., 2010a. Petrogenesis and tectonic significance of the similar to 850 Ma Gangbian alkaline complex in South China: evidence from in situ zircon U–Pb dating, Hf–O isotopes and whole-rock geochemistry. Lithos 114, 1–15.
Li, X.H., Long, W.G., Li, Q.L., Liu, Y., Zheng, Y.F., Yang, Y.H., Chamberlain, K.R., Wan, D.F., Guo, C.H., Wang, X.C., Tao, H., 2010b. Penglai zircon megacrysts: a potential new working reference material for microbeam determination of Hf–O isotopes and U–Pb age. Geostandards and Geoanalytical Research 34, 117–134.
Li, J.Y., Zhang, J., Qu, J.F., 2012. Amalgamation of North China Craton with Alxa Block in the Late of Early Paleozoic: evidence from sedimentary sequences in the Niushou mountain, Ningxia Hui Autonomous Region, NW China. Geological Review 58, 208–214 (in Chinese with English abstract).
Liu, D.Y., Nutman, A.P., Compston, W., Wu, J.S., Shen, Q.H., 1992. Remnants of ≥3800 Ma crust in the Chinese part of the Sino-Korean Craton. Geology 20, 339–342.
Liu, Y.S., Gao, S., Yuan, H.L., Zhou, L., Liu, X., Wang, X.C., Hua, Z.C., Wang, L.S., 2004. U–Pb zircon ages and Nd, Sr, and Pb isotopes of lower crustal xenoliths from North China Craton: insights on evolution of lower continental crust. Chemical Geology 211, 87–109.
Liu, Y.S., Gao, S., Hu, Z.C., Gao, C.G., Zong, K.Q., Wang, D.B., 2010. Continental and oceanic crust recycling-induced melt-peridotite interactions in the Trans-North China Orogen: U–Pb dating, Hf isotopes and trace elements in zircons from mantle xenoliths. Journal of Petrology 51, 537–571.
Liu, C.Z., Wu, F.Y., Chung, S.L., Li, Q.L., Sun, W.D., Ji, W.Q., 2014. A 'hidden' 18O-enriched reservoir in the sub-arc mantle. Scientific Reports 4, 4232. http://dx.doi.org/10.1038/srep04232.
Ludwig, K.R., 2003. Users Manual for Isoplot 3.00: A Geochronological Toolkit for Microsoft Excel. 4. Berkeley Geochronology Center, Special, Publication.
Macpherson, C.G., Dreher, S.T., Thirlwall, M.F., 2006. Adakites without slab melting: high pressure differentiation of island arc magma, Mindanao, the Philippines. Earth and Planetary Science Letters 243, 581–593.
Martin, H., Smithies, R.H., Rapp, R., Moyen, J.F., Champion, D., 2005. An overview of adakite, tonalite–trondhjemite–granodiorite (TTG), and sanukitoid: relationships and some implications for crustal evolution. Lithos 79, 1–24.
Martin, E., Bindeman, I., Grove, T.L., 2011. The origin of high-Mg magmas in Mt Shasta and Medicine Lake volcanoes, Cascade Arc (California): higher and lower than mantle oxygen isotope signatures attributed to current and past subduction. Contributions to Mineralogy and Petrology 162, 945–960.
Meert, J.G., 2012. What's in a name? The Columbia (Paleopangea/Nuna) supercontinent. Gondwana Research 21, 987–993.
Middlemost, E.A.K., 1994. Naming materials in the magma/igneous rock system. Earth-Science Reviews 37, 215–224.
Moyen, J.F., 2009. High Sr/Y and La/Yb ratios: the meaning of the "adakitic signature". Lithos 112, 556–574.
Muir, R.J., Weaver, S.D., Bradshaw, J.D., Eby, G.N., Evans, J.A., 1995. The Cretaceous Separation Point batholith, New Zealand: granitoid magmas formed by melting of mafic lithosphere. Journal of the Geological Society 152, 689–701.
Nance, R.D., Murphy, J.B., Santosh, M., 2014. The supercontinent cycle: a retrospective essay. Gondwana Research 25, 4–29.
NMBGMR (Nei Mongol Bureau of Geology and Mineral Resources), 1991. Regional Geology of Nei Mongol Autonomous Region. Geological Publishing House, Beijing (725 pp. (in Chinese with English abstract)).
Peccerillo, A., Taylor, S.R., 1976. Geochemistry of Eocene calc-alkaline volcanic rocks from the Kastamonu area, Northern Turkey. Contributions to Mineralogy and Petrology 58, 63–81.
Peck, W.H., Valley, J.W., Corriveau, L., Davidson, A., McLelland, J., Farber, D.A., 2004. Oxygen-isotope constraints on terrane boundaries and origin of 1.18–1.13 Ga granitoids in the southern Grenville province. In: Tollo, R.P., Corriveau, L., McLelland, J., Bartholomew, M.J. (Eds.), Proterozoic Tectonic Evolution of the Grenville Orogen in North America: Boulder, Colorado. Geological Society of America Memoir 197, pp. 163–182.
Peng, P., Bleeker, W., Ernst, R.E., Soderlund, U., McNicoll, V., 2011. U–Pb baddeleyite ages, distribution and geochemistry of 925 Ma mafic dykes and 900 Ma sills in the North China Craton: evidence for a Neoproterozoic mantle plume. Lithos 127, 210–221.
Petford, N., Atherton, M., 1996. Na-rich partial melts from newly underplated basaltic crust: the Cordillera Blanca Batholith, Peru. Journal of Petrology 37, 1491–1521.
Rapp, R.P., Watson, E.B., 1995. Dehydration melting of metabasalt at 8–32 kbar: implications for continental growth and crust–mantle recycling. Journal of Petrology 36, 891–931.
Rapp, R.P., Shimizu, N., Norman, M.D., Applegate, G.S., 1999. Reaction between slab-derived melts and peridotite in the mantle wedge: experimental constraints at 3.8 GPa. Chemical Geology 160, 335–356.
Richards, J.R., Kerrich, R., 2007. Special paper: adakite-like rocks: their diverse origins and questionable role in metallogenesis. Economic Geology 102, 537–576.
Roberts, N.M.W., 2013. The boring billion?—Lid tectonics, continental growth and environmental changes associated with the Columbia supercontinent. Geoscience Frontiers 4, 681–691.
Roberts, N.M.W., Slagstad, T., Parrish, R.R., Norry, M.J., Marker, M., Horstwood, M.S.A., 2013. Sedimentary recycling in arc magmas: geochemical and U–Pb–Hf–O constraints on the Mesoproterozoic Suldal Arc, SW Norway. Contributions to Mineralogy and Petrology 165, 507–523.
Rogers, J.J.W., Santosh, M., 2009. Tectonics and surface effects of the supercontinent Columbia. Gondwana Research 15, 373–380.
Rooney, T.O., Franceschi, P., Hall, C.M., 2011. Water-saturated magmas in the Panama Canal region: a precursor to adakite-like magma generation? Contributions to Mineralogy and Petrology 161, 373–388.
Sen, C., Dunn, T., 1994. Dehydration melting of a basaltic composition amphibolite at 1.5 and 2.0 GPa: implications for the origin of adakites. Contributions to Mineralogy and Petrology 117, 394–409.
Skjerlie, K.P., Patiño Douce, A.E., 2002. The fluid-absent partial melting of a zoisite bearing quartz eclogite from 1.0 to 3.2 GPa: implications for melting in thickened continental crust and for subduction-zone processes. Journal of Petrology 43, 291–314.
Springer, W., Seck, H.A., 1997. Partial fusion of basic granulites at 5 to 15 kbar: implications for the origin of TTG magmas. Contributions to Mineralogy and Petrology 127, 30–45.
Streck, M.J., Leeman, W.P., Chesley, J., 2007. High-magnesian andesite from Mount Shasta: a product of magma mixing and contamination, not a primitive mantle melt. Geology 35, 351–354.
Su, Y.P., Zheng, J.P., Griffin, W.L., Zhao, J.H., O'Reilly, S.Y., Tang, H., Ping, X.Q., Xiong, Q., 2013. Petrogenesis and geochronology of Cretaceous adakitic, I- and A-type granitoids in the NE Yangtze block: constraints on the eastern subsurface boundary between the North and South China blocks. Lithos 175–176, 333–350.
Sun, S.S., McDonough, W.F., 1989. Chemical and isotopic systematics of oceanic basalt: implications for mantle composition and processes. In: Sanders, A.D., Norry, M.J. (Eds.), Magmatism in the Ocean Basins. Geological Society Special Publication 42, pp. 528–548.
Teixeira, W., D'Agrella-Filho, M.S., Ernst, R.E., Hamilton, M.A., Girardi, V.A.V., Mazzucchelli, M., Bettencourt, J.S., 2013. U–Pb (ID-TIMS) baddeleyite ages and paleomagnetism of 1.79 and 1.50 Ga tholeiitic dyke swarms, and position of the Rio de la Plata craton within the Columbia supercontinent. Lithos 174, 157–174.
Valley, J.W., Lackey, J.S., Cavosie, A.J., Clechenko, C.C., Spicuzza, M.J., Basei, M.A.S., Bindeman, I.N., Ferreira, V.P., Sial, A.N., King, E.M., Peck, W.H., Sinha, A.K., Wei, C.S., 2005. 4.4 billion years of crustal maturation: oxygen isotope ratios of magmatic zircon. Contributions to Mineralogy and Petrology 150, 561–580.
Wang, Y.Q., 2012. Sedimentary Facies Characteristics of the Carboniferous in the Bayanhot Basin. (M.S. thesis), Chengdu University of Technology, Chengdu (71 pp.).
Wang, Q., McDermott, F., Xu, J.F., Bellon, H., Zhu, Y.T., 2005. Cenozoic K-rich adakitic volcanic rocks in the Hohxil area, northern Tibet: lower-crustal melting in an intracontinental setting. Geology 33, 465–468.
Wang, Q., Xu, J.F., Jian, P., Bao, Z.W., Zhao, Z.H., Li, C.F., Xiong, X.L., Ma, J.L., 2006a. Petrogenesis of adakitic porphyries in an extensional tectonic setting, Dexing, South China: implications for the genesis of porphyry copper mineralization. Journal of Petrology 47, 119–144.
Wang, X.C., Liu, Y.S., Liu, X.M., 2006b. Mesozoic adakites in the Lingqiu Basin of the central North China Craton: partial melting of underplated basaltic lower crust. Geochemical Journal 40, 447–461.
Wang, Q., Wyman, D., Zhao, Z., Xu, J., Bai, Z., Xiong, X., Dai, T., Li, C., Chu, Z., 2007a. Petrogenesis of Carboniferous adakites and Nb-enriched arc basalts in the Alataw area, northern Tianshan Range (western China): implications for Phanerozoic crustal growth in the Central Asia orogenic belt. Chemical Geology 236, 42–64.
Wang, Q., Wyman, D.A., Xu, J.F., Jian, P., Zhao, Z.H., Li, C.F., Xu, W., Ma, J.L., He, B., 2007b. Early Cretaceous adakitic granites in the Northern Dabie Complex, central China: implications for partial melting and delamination of thickened lower crust. Geochimica et Cosmochimica Acta 71, 2609–2636.
Wang, Q., Wyman, D.A., Xu, J.F., Wan, Y.S., Li, C.F., Zi, F., Jiang, Z.Q., Qiu, H.N., Chu, Z.Y., Zhao, Z.H., Dong, Y.H., 2008a. Triassic Nb-enriched basalts, magnesian andesites, and adakites of the Qiangtang terrane (Central Tibet): evidence for metasomatism by slab-derived melts in the mantle wedge. Contributions to Mineralogy and Petrology 155, 473–490.
Wang, Q., Wyman, D.A., Xu, J.F., Dong, Y.H., Vasconcelos, P.M., Pearson, N., Wan, Y.S., Dong, H., Li, C.F., Yu, Y.S., Zhu, T.X., Feng, X.T., Zhang, Q.Y., Zi, F., Chu, Z.Y., 2008b. Eocene melting of subducting continental crust and early uplifting of central Tibet: evidence from central-western Qiangtang high-K calc-alkaline andesites, dacites and rhyolites. Earth and Planetary Science Letters 272, 158–171.

Wang, W., Liu, S.W., Santosh, M., Zhang, L.F., Bai, Z., Zhao, Y., Zhang, S.H., Guo, R.R., 2015. 1.23 Ga mafic dykes in the North China Craton and their implications for the reconstruction of the Columbia supercontinent. Gondwana Research 27 (4), 1407–1418.
Wiedenbeck, M., Hanchar, J.M., Peck, W.H., Sylvester, P., Valley, J., Whitehouse, M., Kronz, A., Morishita, Y., Nasdala, L., Fiebig, J., Franchi, I., Girard, J.P., Greenwood, R.C., Hinton, R., Kita, N., Mason, P.R.D., Norman, M., Ogasawara, M., Piccoli, R., Rhede, D., Satoh, H., Schulz-Dobrick, B., Skar, O., Spicuzza, M.J., Terada, K., Tindle, A., Togashi, S., Vennemann, T., Xie, Q., Zheng, Y.F., 2004. Further characterisation of the 91500 zircon crystal. Geostandards and Geoanalytical Research 28, 9–39.
Wong, J., Sun, M., Xing, G.F., Li, X.H., Zhao, G.C., Wong, K., Wu, F.Y., 2011. Zircon U–Pb and Hf isotopic study of Mesozoic felsic rocks from eastern Zhejiang, South China: geochemical contrast between the Yangtze and Cathaysia blocks. Gondwana Research 19, 244–259.
Wu, F.Y., Zhao, G.C., Wilde, S.A., Sun, D.Y., 2005. Nd isotopic constraints on crustal formation in the North China Craton. Journal of Asian Earth Sciences 24, 523–545.
Wu, F.Y., Yang, Y.H., Xie, L.W., Yang, J.H., Xu, P., 2006. Hf isotopic compositions of the standard zircons and baddeleyites used in U–Pb geochronology. Chemical Geology 234, 105–126.
Wu, F.Y., Zhang, Y.B., Yang, J.H., Xie, L.W., Yang, Y.H., 2008a. Zircon U–Pb and Hf isotopic constraints on the Early Archean crustal evolution in Anshan of the North China Craton. Precambrian Research 167, 339–362.
Wu, F.Y., Xu, Y.G., Gao, S., Zheng, J.P., 2008b. Lithospheric thinning and destruction of the North China Craton. Acta Petrologica Sinica 24, 1145–1174.
Wu, F.Y., Ji, W.Q., Wang, J.G., Liu, C.Z., Chung, S.L., Clift, P., 2014. Zircon U–Pb and Hf isotopic constraints on the onset time of India–Asia collision. American Journal of Science 314, 548–579.
Xie, L.W., Zhang, Y.B., Zhang, H.H., Sun, J.F., Wu, F.Y., 2008. In situ simultaneous determination of trace elements, U–Pb and Lu–Hf isotopes in zircon and baddeleyite. Chinese Science Bulletin 53, 1565–1573.
Xiong, B.X., Chen, W.X., Chen, W.L., Cao, X.Y., 2001. Formation and evolution of the Bayanhaote prototype basins. Petroleum Geology & Experiment 23, 19–22 (in Chinese with English abstract).
Yin, A., Harrison, T.M., 2000. Geologic evolution of the Himalayan–Tibetan orogen. Annual Review of Earth and Planetary Sciences 28, 211–280.
Yuan, X.Q., Geng, G.C., 1992. Discovery of Paleozoic sediments in east Bayanhot basin and its tectonic significance. Oil & Gas Geology 13, 381–389 (in Chinese with English abstract).
Yuan, W., Yang, Z.Y., 2015a. The Alashan Terrane was not part of North China by the Late Devonian: evidence from detrital zircon U–Pb geochronology and Hf isotopes. Gondwana Research 27 (3), 1270–1282.
Yuan, W., Yang, Z.Y., 2015b. The Alashan Terrane did not amalgamate with North China block by the Late Permian: evidence from Carboniferous and Permian paleomagnetic results. Journal of Asian Earth Sciences http://dx.doi.org/10.1016/j.jseaes.2014.02.010.
Zhai, M.G., Santosh, M., 2011. The early Precambrian odyssey of the North China Craton: a synoptic overview. Gondwana Research 20, 6–25.
Zhai, M.G., Bian, A.G., Zhao, T.P., 2000. The amalgamation of the supercontinent of North China Craton at the end of Neo-Archaean and its breakup during late Palaeoproterozoic and Meso-Proterozoic. Science in China Series D-Earth Sciences 43, 219–232.
Zhang, H.X., Sun, D.Z., Zhu, B.Q., Tu, X.L., 2000. Pb, Nd isotopic study of Proterozoic metamorphic sediments in North Jiangxi and its tectonic significance. Regional Geology of China 19, 66–71.
Zhang, H.F., Xiao, L., Zhang, L., Yuan, H.L., Jin, L.L., 2007. Geochemical and Pb–Sr–Nd isotopic compositions of Indosinian granitoids from the Bikou block, northwest of the Yangtze plate: constraints on petrogenesis, nature of deep crust and geodynamics. Science in China Series D: Earth Sciences 50, 972–983.
Zhang, J., Li, J.Y., Liu, J.F., Feng, Q.W., 2011. Detrital zircon U–Pb ages of Middle Ordovician flysch sandstones in the western Ordos margin: new constraints on their provenances, and tectonic implications. Journal of Asian Earth Sciences 42, 1030–1047.
Zhang, J., Li, J.Y., Liu, J.F., Li, Y.F., Qu, J.F., Feng, Q.W., 2012. The relationship between the Alxa Block and the North China Plate during the Early Peleozoic:new information from the Middle Ordovician detrital zircon ages in the eastern Alxa Block. Acta Petrologica Sinica 28, 2912–2934 (in Chinese with English abstract).
Zhang, J.X., Gong, J.H., Yu, S.Y., Li, H.K., Hou, K.J., 2013a. Neoarchean–Paleoproterozoic multiple tectonothermal events in the western Alxa block, North China Craton and their geological implication: evidence from zircon U–Pb ages and Hf isotopic composition. Precambrian Research 235, 36–57.
Zhang, J.X., Yu, S.Y., Gong, J.H., Li, H.K., Hou, K.J., 2013b. The latest Neoarchean–Paleoproterozoic evolution of the Dunhuang block, eastern Tarim craton, northwestern China: evidence from zircon U–Pb dating and Hf isotopic analyses. Precambrian Research 226, 21–42.
Zhang, J., Li, J.Y., Xiao, W.X., Wang, Y.N., Qi, W.H., 2013c. Kinematics and geochronology of multistage ductile deformation along the eastern Alxa block, NW China: new constraints on the relationship between the North China Plate and the Alxa block. Journal of Structural Geology 57, 38–57.
Zhang, J., Li, J.Y., Liu, J.F., Li, Y.F., Qu, J.F., Zhang, Y.P., 2013d. LA-ICP-MS U–Pb ages of pillow lava basalts in southwestern Langshan, Inner Mongolia and their implication. Geological Bulletin of China 32, 287–296 (in Chinese with English abstract).
Zhao, G.C., 2014. Precambrian Evolution of the North China Craton. Elsevier, Amsterdam (194 pp.).
Zhao, G.C., Cawood, P.A., 2012. Precambrian geology of China. Precambrian Research 222–223, 13–54.
Zhao, G.C., Zhai, M.G., 2013. Lithotectonic elements of Precambrian basement in the North China Craton: review and tectonic implications. Gondwana Research 23, 1207–1240.
Zhao, G.C., Sun, M., Wilde, S.A., 2002. Review of global 2.1–1.8 Ga orogens: implications for a Pre-Rodinia supercontinent. Earth-Science Reviews 59, 125–162.
Zhao, G.C., Sun, M., Wilde, S.A., Li, S.Z., 2004. A Paleo-Mesoproterozoic supercontinent: assembly, growth and breakup. Earth Science Reviews 67, 91–123.
Zhao, G.C., Sun, M., Wilde, S.A., Li, S.Z., 2005. Late Archean to Paleoproterozoic evolution of the North China Craton: key issues revisited. Precambrian Research 136, 177–202.
Zhao, G.C., Cawood, P.A., Li, S.Z., Wilde, S.A., Sun, M., Zhang, J., He, Y.H., Yin, C.Q., 2012. Amalgamation of the North China Craton: key issues and discussion. Precambrian Research 222–223, 55–76.
Zheng, Y.F., Xiao, W.J., Zhao, G., 2013. Introduction to tectonics of China. Gondwana Research 23, 1189–1206.
Zhu, R.K., Meng, X.H., Ge, M., 1994. Mixed deep-water gravity current sedimentary sequences of middle-Ordovician series in the east margin of Bayanhaote basin. Acta Sedimentologica Sinica 12, 77–85 (in Chinese with English abstract).
Zhu, B.Q., Chen, Y.W., Peng, J.H., 2001. Lead isotope geochemistry of the urban environment in the Pearl River Delta. Applied Geochemistry 16, 409–417.
Zi, J.W., Cawood, P.A., Fan, W.M., Tohver, E., Wang, Y.J., McCuaig, T.C., 2012. Generation of Early Indosinian enriched mantle-derived granitoid pluton in the Sanjiang Orogen (SW China) in response to closure of the Paleo-Tethys. Lithos 140–141, 166–182.